SI Appendix for the paper:

NADPH-dependent extracellular superoxide production is vital to photophysiology in the marine diatom *Thalassiosira oceanica*

Julia M. Diaz, Sydney Plummer, Colleen M. Hansel, Peter F. Andeer, Mak A. Saito, Matthew R. McIlvin

Experimental Methods

Culture conditions, growth monitoring, and cell counts

Thalassiosira oceanica CCMP1005 was obtained from the National Center for Marine Algae and Microbiota (NCMA), Bigelow Laboratories, East Boothbay, Maine. *T. oceanica* was maintained in autoclaved (121°C, 20 min) f/2 media (1) prepared using filtered (0.2 μm) natural seawater. *T. oceanica* was cultivated on a 14h:10h light:dark cycle (340 μmol photons m^{-2} s^{-1}) at either 18°C or 23°C. Culture growth was monitored daily by measuring *in vivo* chlorophyll fluorescence with an AquaFluor handheld fluorometer (Turner Designs) or a 10-AU benchtop fluorometer (Turner Designs). For cell counts, culture samples were preserved in Lugol's solution (2% final concentration) and enumerated using a hemocytometer counting chamber or preserved in glutaraldehyde (0.5% final concentration) and counted on a Guava EasyCyte HT flow cytometer (Millipore). Instrument-specific beads were used to calibrate the cytometer. Samples were analyzed at a low flow rate (0.24 μL s^{-1}) for 3 min, and cells were counted based on diagnostic forward scatter vs. red fluorescence signals. The original *T. oceanica* culture obtained from the NCMA was certified axenic, and the Diaz lab routinely checks that the culture is free of bacterial and fungal contamination by inoculating 200 μL into 5 mL of marine broth and incubating in the dark for a period of several days.

Superoxide dismutase experiment

In an experiment conducted in May and June 2018, *T. oceanica* was grown in the presence of superoxide dismutase (SOD, Millipore Sigma). Cultures (25 mL) were inoculated at an initial concentration of ~ 1×10^5 cells mL^{-1}. Cultures received daily additions (125 μL) of the following: 50 U mL^{-1} SOD (final concentration), dialyzed SOD, and deionized water. Dialyzed SOD was prepared via diafiltration through a 10 kDa Amicon ultrafiltration device (Millipore), according to the manufacturer's instructions. To calculate specific growth rates (d^{-1}), daily *in vivo* fluorescence (IVF) was normalized to the value obtained on day 0. Then the following equation was applied over the log linear portion of growth ($R^2 > 0.98$ in all cultures):

$$d^{-1} = \frac{\ln\left(\frac{IVF_f}{IVF_i}\right)}{\Delta t}$$

where IVF_f and IVF_i are the normalized *in vivo* fluorescence values on the final and initial day of exponential growth, respectively, and Δt is the number of days of exponential growth.

Preparation of concentrated exoprotein samples

T. oceanica cell-free filtrates were harvested and concentrated in three separate experiments conducted in March 2014, November 2014, and June 2016 (Figs. S2 and S3). To generate cell-free filtrate samples, 2L of *T. oceanica* were cultivated in acid-washed Fernbach flasks at 23°C. In mid-exponential growth, cultures were centrifuged (3000×g, 20min, 4°C), decanted, and centrifuged again (3000×g, 20min, 4°C) before being filtered (0.2µm, PES). The cell-free filtrates were then concentrated to ~20-100 mL via tangential flow filtration (TFF) using a Pellicon-2 Mini ultrafiltration system (Millipore Sigma) equipped with a composite regenerated cellulose membrane (10kDa molecular weight cut-off). TFF samples were diafiltered and concentrated further (0.5 mL) into 20 mM Tris (pH=8.0) using a 10 kDa Centricon® Plus-70 centrifugal filter device (Millipore Sigma), according to the manufacturer's instructions. The ultrafiltered biological triplicates from one experiment (March 2014) were pooled and further concentrated using a 10kDa Amicon Ultra-0.5 centrifugal filter device (Millipore Sigma), according to the manufacturer's instructions.

Superoxide production by *T. oceanica* concentrated exoproteins and ScGR

NADPH-dependent superoxide production by *Saccharomyces cerevisiae* glutathione reductase (ScGR; Millipore Sigma G3664) and *T. oceanica* exoproteins from November 2014 (Fig. S2) was measured using a microplate assay based on the reaction between superoxide and the probe nitroblue tetrazolium (NBT), which produces the chromogenic monoformazan (MF^+) ion (2).

For ScGR, the enzyme was first dialyzed into 5mM Tris (pH=8) using an Amicon Ultra-0.5 centrifugal filter device (Millipore Sigma), according to the manufacturer's instructions and then incubated with formaldehyde following procedures consistent with Schneider et al. (2016) ref. (3). Briefly, ScGR was incubated at 4°C for two hours in 5mM Tris amended with nothing or with 4% formaldehyde (final concentration) at pH 5 or 8. To remove the formaldehyde, each ScGR treatment was then dialyzed into 5mM Tris (pH=8), as above. These samples were incubated for an hour at 4°C prior to analysis.

ScGR and concentrated *T. oceanica* exoprotein samples were diluted in 5mM Tris (pH=8) and loaded into a transparent 96-well microplate. All wells were amended with 40µM DTPA and 40µM NBT (final concentrations). The effect of several potential stimulants and inhibitors were assessed, including NADPH (200µM), $NADP^+$ (200µM), SOD (1X = 50 U mL^{-1} or 2X = 100 U mL^{-1}), GSSG (200µM), GSH (200µM), DPI (50µM) dissolved in 1.3% DMSO, and 1.3% DMSO (final concentrations). A subset of *T. oceanica* concentrated exoprotein samples was also boiled (100°C, 30min) prior to loading in the microplate. Triplicate negative controls lacking any protein sample were prepared for each treatment and analyzed in the same microplate. Final reaction volumes were uniform in order to avoid inconsistencies in the final calculation of superoxide production (see below).

Absorbance readings at 530nm (MF^+) and 720nm (background) were collected every 2.5 - 15min for 1 - 4 hours on a SpectraMax multimode plate reader (Molecular Devices). At every time point, the absorbance signal at 720nm was subtracted from the absorbance at 530nm. The average background-corrected absorbance of protein-free negative controls was then subtracted at every time point in order to correct for any abiotic signal produced in the absence of protein samples. The linear increase in corrected absorbance over time was determined over the incubation period (typically, $R > 0.95$). Absorbance was converted to moles of MF^+ produced based on the molar absorptivity of MF^+ at 530nm and pH=8.0 (20,000 M^{-1} cm^{-1}) and the empirical path length (0.6 cm). Detection limits calculated as three times the standard deviation of replicate protein-free blanks typically ranged from 0.02 – 0.2 μmol MF^+ L^{-1} hr^{-1}, depending on the treatment. Volume-normalized rates of MF^+ production in ScGR and exoprotein samples were between three- and three hundred-fold higher than these detection limits. NBT can be reduced to MF^+ independently of superoxide, as reflected by non-zero rates of MF^+ production in the presence of SOD. To determine NADPH-dependent rates of superoxide production, the rate of MF^+ production in the presence of NADPH and SOD was therefore subtracted and then the reaction stoichiometry of MF^+:O_2^- (1:2) was applied (2). Reported rates of MF^+ and superoxide production were normalized to total protein content, as determined below.

Determination of total protein content

Total protein levels were determined in concentrated exoproteins using a Bradford Protein Assay Kit with bovine serum albumin (BSA) as the standard (Bio-Rad). Samples were analyzed according to the manufacturer's instructions for a microplate-based assay. Briefly, samples were diluted in 5 mM Tris (pH=8.0) in a 96-well transparent microplate, mixed and reacted with the colorimetric dye for ten minutes, and analyzed for absorbance at 595 nm on a SpectraMax multimode plate reader (Molecular Devices). BSA calibration standards ranged from 1.25 – 20 μg mL^{-1}. Analytical precision was typically < 3%, and the detection limit, defined as three times the standard deviation of replicate blanks, was 0.5 μg mL^{-1}.

Native polyacrylamide gel electrophoresis (PAGE), in-gel activity assay, and protein digestion

Concentrated filtrate samples were mixed with non-denaturing LDS loading buffer (Thermo Scientific) and loaded directly into 4-20% pre-cast Tris-Glycine polyacrylamide gels alongside a pre-stained protein ladder (Thermo Scientific). Gels were run in a MiniProtean Cell (BioRad) using non-denaturing running buffer (14.4 g L^{-1} glycine, 3 g L^{-1} Tris base, pH=8.3) at 185V for 55min.

After native PAGE, gels were rinsed three times in HPLC-grade water and incubated following the procedure of Andeer et al. (4). Briefly, gels were reacted with gentle mixing in 5mM Tris, (pH=8) supplemented with 40μM DTPA and 40μM NBT with or without the addition of 150μM NADPH or 50 U mL^{-1} SOD, as indicated. Gels were allowed to react overnight. Activity bands were excised with disposable scalpels in a laminar flow hood, and proteins were digested using an in-gel tryptic digestion kit (Thermo Scientific), according to the manufacturer's instructions.

Peptide fingerprinting of digested NBT gel bands

Peptide samples were analyzed via liquid chromatography tandem mass spectrometry (LC/MS/MS). Samples were run using slightly different LC/MS/MS protocols, depending on when they were generated (Fig. S3). The first biological replicate (X), a pooled sample generated in March 2014, was analyzed at the WHOI FT-MS facility, according to methods outlined in Andeer et al. (4). Briefly, sample X was injected twice (i.e., technical duplicates) onto a 0.3 × 150mm Magic C18AQ 3μm, 200Å column (Bruker-Michrom) and eluted (5 μL min^{-1}) with a gradient of 0.1% formic acid in water and 0.1% formic acid in acetonitrile by the following steps: (1) 4% B (0-5min), (2) linear increase to 45% B (5-82 min), (3) linear increase to 90% B (82-85 min), (4) 90% B (85-100 min), (5) return to 4% B (100-105 min). Column fractions from sample X were analyzed on a linear trap quadrupole (LTQ XL, Thermo Scientific), which conducted tandem MS on the top five ions within a mass-to-charge ratio of 400.00 to 2000.00 using data-dependent secondary MS settings with a 30s dynamic exclusion window.

Biological replicates Y and Z were analyzed in the Saito Lab (Fig. S3) via LC/MS/MS using a Michrom Advance HPLC system with reverse phase chromatography coupled to a Thermo Scientific Q-Exactive Orbitrap mass spectrometer with a Michrom Advance CaptiveSpray source. Each sample was concentrated onto a trap column (0.2 x 10 mm ID, 5 μm particle size, 120 Å pore size, C18 Reprosil-Gold, Dr. Maisch GmbH) and rinsed with 100 μL 0.1% formic acid, 2% acetonitrile (ACN), 97.9% water before gradient elution through a reverse phase C18 column (0.1 x 150 mm ID, 3 μm particle size, 120 Å pore size, C18 Reprosil-Gold, Dr. Maisch GmbH) at a flow rate of 500 nL/min. The chromatography consisted of a nonlinear 90 min gradient from 5% to 95% buffer B, where A was 0.1% formic acid in water and B was 0.1% formic acid in ACN (all solvents were Fisher Optima grade). The mass spectrometer monitored MS1 scans from 380 m/z to 1580 m/z at 70K resolution. MS2 scans were performed on the top 10 ions with an isolation window of 1.6 m/z and a 15 second exclusion time.

Mass spectra were mapped to the reference database in Proteome Discoverer (version 2.2, Thermo) using Proteome Discoverer's SEQUEST HT algorithm (Thermo Scientific) with a parent tolerance of 10 ppm and a fragment tolerance of 0.02 Da. The *in silico* tryptic peptide database was assembled from the translated whole genome of *T. oceanica* (NCBI Bioproject PRJNA36595) and a list of common contaminants, such as human keratin. Proteome Discoverer automatically generates the reversed (decoy) sequences for false discovery rate (FDR) analysis. Identification criteria consisted of a peptide threshold of 95% and protein threshold of 1.0% FDR, corresponding to a protein FDR of 0.6%. Protein matches were also filtered to exclude hits with fewer than two unique peptide identifications. For sample X, results from technical replicates were added together. Gene ontology (GO) annotations were integrated into results using the ProteinCenter Annotation node.

Protein sequence analysis

BLASTP

Several marine phytoplankton genomes were searched with a variety of query sequences using the National Center for Biotechnology Information (NCBI) online BLASTP suite with default parameters (https://blast.ncbi.nlm.nih.gov). Genomes searched included *T. oceanica* CCMP1005 (TaxID: 159749), *Emiliania huxleyi* CCMP1516 (TaxID: 2903), *Ostreococcus tauri* (TaxID:

70448), *Thalassiosira pseudonana* CCMP1335 (TaxID:35128), *Micromonas pusilla* CCMP1545 (TaxID:38833), *Phaeodactylum tricornutum* CCAP 1055/1 (TaxID:556484), *Fragilariopsis cylindrus* CCMP1102 (TaxID:186039), and *Symbiodinium microadriaticum* CCMP2467 (TaxID:2951). Query sequences included a broad phylogenetic diversity of Nox enzymes (5): canonical NADPH oxidase (Nox) and Dual oxidase (Duox) from human (NCBI accession AAG17121 and AAF78954, respectively), and respiratory burst oxidases (Rbo) from the green alga *Chlamydomonas reinhardtii* (Rbo1: XP_001691855.1; Rbo2: XP_001691856.1), the red macro-alga *Chondrus crispus* (AAZ73480), and the flowering plant *Arabidopsis thaliana* (AAC39476). Representative phytoplankton genomes were also searched with *T. oceanica* GR1 (EJK45974). Putative glutathione reductase sequences were identified in the *T. oceanica* genome by querying with sequences of structurally characterized flavoenzyme disulfide reductases: glutathione reductase from *Homo sapiens* (Protein Data Bank 3GRS), *Saccharomyces cerevisiae* (2HQM), and *Escherichia coli* (1GER), and trypanothione reductase from *Trypanosoma cruzi* (1AOG).

In order to investigate the identity of the *T. oceanica* GR's as putative glutathione reductases, the UniProtKB database was searched online via BLASTP analysis (https://www.uniprot.org/blast/) using ToGR1 and ToGR2 as query sequences (Genbank accession EJK45974 and EJK71311, respectively). The top hits with 3D structural data were determined by selecting the Protein Data Bank (PDB) database, and results were filtered to include reviewed records only.

The Ocean Gene Atlas database contains metagenomic data from diverse oceanic environments across the world, which were obtained during the *Tara* Oceans expedition (6, 7). The Marine Atlas of Tara Oceans Unigenes (MATOUv1) was searched for putative homologs of ToGR1 using BLASTP analysis with an E-value threshold $\leq 1 \times 10^{-10}$. Hits were limited to only those found within the major phytoplankton groups (Stramenopiles, Dinophyceae, Haptophyceae, and Chlorophyta). Results from all size fractions were pooled: 0.8 – 5 µm, 5 – 20 µm, 20 – 180 µm, and 180 – 2000 µm. Figures were generated using Plotly (https://plot.ly/).

Multiple sequence alignment, sequence annotation, and phylogenetic tree

Structure-based multiple sequence alignment of ToGR1, ToGR2, and reference flavoprotein disulfide reductases was performed using PROMALS3D (http://prodata.swmed.edu/promals3d/promals3d.php) ref. (8). Sequence data from reference proteins were extracted from structure files by entering protein structures by their Protein Data Bank (PDB) ID. Reference proteins consisted of glutathione reductase (GR) from *Homo sapiens* (PDB ID 3GRS), *Saccharomyces cerevisiae* (2HQM), and *Escherichia coli* (1GER), trypanothione reductase (TR) from *Trypanosoma cruzi* (1AOG), and thioredoxin reductase from *Homo sapiens* (3QFA).

The multiple sequence alignment was annotated using protein structural information from human GR (9-15), yeast GR (16), *E. coli* GR (17), and *T. cruzi* TR (18-20). In particular, we looked for the active site disulfide (10, 16-18), two conserved motifs for FAD binding (Gly-X-Gly-X-X-Gly and Thr-X-X-X-X-h-y-h-h-Gly-Asp, where X is any amino acid, h is a small nonpolar amino acid, and y is an aromatic residue) ref (18), a crucial region for NADPH binding (11), and key amino acids conferring substrate specificity, including Trp22 and Met114 forming the hydrophobic patch of TR, as well as three additional amino acids that help confer substrate specificity according to site-directed mutagenesis (15, 18). We also investigated sequence

features corresponding to intersubunit binding (16), including the intersubunit C-terminal extensions present in TR and *E. coli* GR (19, 20). Putative transmembrane binding and signal peptide domains identified by the protein topology prediction methods below were also indicated in the annotated sequence alignment.

To construct the phylogenetic tree, the aligned sequences were analyzed in SeaView (http://doua.prabi.fr/software/seaview) using the neighbor joining method with 1000 bootstrap replicates ref. (21). The tree was then edited using the interactive Tree of Life (iTOL; https://itol.embl.de/) ref. (22).

Prediction of signal peptides, transmembrane binding topology, and enzyme localization

To predict protein localization and determine the presence of putative transmembrane binding sites and signal peptide domains, ToGR1, ToGR2, and related enzyme sequences were analyzed with several online tools. Analyzed sequences included GR from *Homo sapiens* (PDB ID 3GRS), *Saccharomyces cerevisiae* (2HQM), and *Escherichia coli* (1GER), and TR from *Trypanosoma cruzi* (1AOG), as well as putative ToGR1 homologs from representative marine phytoplankton genomes (see Table S11). To reveal potential signal peptides, sequences were analyzed with PrediSi using default parameters after selecting the appropriate organism group (www.predisi.de) ref. (23). The tmap prediction tool was used to search for potential transmembrane domains using default parameters (http://www.bioinformatics.nl/cgi-bin/emboss/tmap) ref. (24), and the potential presence of transmembrane domains and signal peptides was also assessed with Polyphobius using default settings (http://phobius.sbc.su.se/poly.html) ref (25). Protein localization was performed with ProtComp version 9.0 by Softberry (http://www.softberry.com). The *T. oceanica* GRs and other phytoplankton sequences were analyzed using the ProtComp module for plant proteins, whereas *H. sapiens* and *S. cereviseae* GRs were analyzed using the Animal/Fungi version, and *E. coli* GR was analyzed with the bacterial version.

Extracellular superoxide production by whole cells

Superoxide was quantified using a flow-through analytical system (FeLume, Waterville Analytical) via reaction with the chemiluminescent probe methyl *Cypridina* luciferin analog (MCLA), as previously described (3, 26-28). Instrument calibration was performed using standard solutions of potassium superoxide (KO_2). First, a clean syringe filter (0.2 μm) was placed in the sample line to mimic conditions used in experiments with *T. oceanica* (see below). The inline filter was continuously flushed (2 mL min^{-1}) with a buffered carrier solution (20 mM phosphate, pH=8.0; 260 mM NaCl, 50 mM Na_2SO_4, 10 mM KCl) using a peristaltic pump. Downstream of the syringe filter, the carrier solution mixed with the MCLA reagent (4 μM MCLA, 50μM diethylene-triamine pentaacetic acid (DTPA), 0.1 M MES, pH=6.0) in a spiral flow cell. An adjacent photomultiplier tube (PMT) reported the chemiluminescence signal in real time using a PC interface. The PMT integration time was set between 30 to 100 ms.

The chemiluminescence signal produced from the mixture of the MCLA reagent and the carrier solution in the presence of the syringe filter was allowed to stabilize (≤4% relative standard deviation, RSD). The stable value was averaged over at least one minute and is referred to as the

instrument blank (B_{Inst}). Next, a primary KO_2 stock was immediately prepared by dissolving KO_2 in basic solution (0.03 N NaOH, pH=12.5; 90 μM DTPA). Primary KO_2 stocks were quantified by measuring absorbance at 240 nm before and after the addition of (SOD, final concentration 2 U mL^{-1}) and applying the extinction coefficient of superoxide corrected for the production of hydrogen peroxide at this wavelength and pH (2183 L mol^{-1} cm^{-1}) (29). The time at which the primary stock was quantified (t_0) was recorded. Primary KO_2 stocks (2 μL) were then diluted into aliquots of buffered carrier solution (10 mL) to generate a working standard of known initial superoxide concentration ($[O_2^-]_{t=0}$), typically between 0.1-20 nmol L^{-1}, which was then run on the FeLume. Chemiluminescence signals from this KO_2 spike (L^{KO2}) were recorded as a function of time (t) over at least two minutes of superoxide decay. Chemiluminescence values expected at t_0 ($L_{t=0}^{KO2}$) were determined as the y-intercept of the following linearized pseudo-first order decay equation:

$$\ln(L_{KO2} - B_{Inst}) = \ln(L_{t=0}^{KO2}) - k(t - t_0) \quad (1)$$

Where k is the pseudo-first order decay constant in s^{-1}. The sensitivity (S, counts pM^{-1}) of the analysis was determined as:

$$S = \frac{L_{t=0}^{KO2}}{[O_2^-]_{t=0}} \quad (2)$$

An average of at least three measurements of S were used for each calibration. The sensitivity was typically between 0.28 – 1.83 counts pM^{-1}, depending on the integration time used (Fig. S12). The detection limit in pM, defined as three times the standard deviation of B_{Inst}, was ~10 – 20 pM. Finally, SOD (800 U/L) was added to the carrier solution in order to confirm the specificity of chemiluminescence signal to superoxide production. This SOD blank (B_{SOD}) was usually lower than B_{Inst} by several hundred chemiluminescence counts, indicating the presence of some superoxide in the instrument blank, likely due to MCLA autooxidation.

To assess superoxide production by *T. oceanica*, superoxide was quantified in the effluent of intact cells hosted on an inline syringe filter (0.2 μm). First, B_{Inst} was collected with the empty filter inline. Next, the pump was briefly stopped, the filter was taken offline, cells were gently loaded on the filter with a syringe, and the filter was placed back in line. Resuming the peristaltic pump, the chemiluminescence signal generated from the cell effluent was allowed to stabilize (≤4% RSD), and the stable signal was averaged over at least two minutes (L_{cells}). Finally, SOD (800 U L^{-1}) was added to the carrier solution to quantify the SOD blank in the presence of cells ($B_{cells+SOD}$). As in calibration runs, $B_{cells+SOD}$ was typically lower than B_{Inst} by several hundred chemiluminescence counts.

Unless otherwise noted, superoxide concentrations produced by *T. oceanica* cells ($[O_2^-]_{cells}$, pmol L^{-1}) were calculated according to the following equation:

$$[O_2^-]_{cells} = \frac{(L_{cells} - B_{Inst})}{S} \quad (3)$$

where the analytical sensitivity (S) is in counts pM^{-1}. Rates of net extracellular superoxide production ($P_{O_2^-}$, amol $cell^{-1}$ hr^{-1}) were then calculated as:

$$P^{O_2^-} = \frac{[O_2^-]_{cells} \times F}{N_{cells}} 6 \times 10^4 \quad (4)$$

where F is the flow rate (2 mL min^{-1}), N_{cells} is the total number of cells loaded onto the inline filter, and 6×10^4 is a constant applied for unit conversion. Net extracellular superoxide production rates were measured across growth phases of *T. oceanica* batch cultures using these procedures in September 2015 and July 2018.

Inhibitors and stimulants – A set of experiments were conducted in September 2015 to examine the effect of chemical inhibitors and stimulants on the production of extracellular superoxide by *T. oceanica*. The buffered carrier solution was supplemented with NADPH (200μM), GSSG (200μM), DPI (50μM) dissolved in 0.3% DMSO, or 0.3% DMSO (final concentrations). B_{Inst}, L_{cells}, and $B_{cells+SOD}$ were determined as detailed above for each amended carrier solution. In the presence of a given inhibitor or stimulant, superoxide concentrations produced by *T. oceanica* cells ($[O_2^-]_{cells}$, pmol L^{-1}) were calculated according to equation (3) using a pooled calibration factor generated from multiple observations of KO_2 chemiluminescence in the presence of each inhibitor and stimulant (0.47 counts pM^{-1}). The inhibitors and stimulants did not alter superoxide calibration factors generated from the unamended carrier solution (Fig. S10). Net rates of extracellular superoxide production in the presence of each inhibitor and stimulant were calculated according to equation 4.

Superoxide irradiance curve – In another set of experiments conducted in July 2018, extracellular superoxide production by *T. oceanica* was examined under a broad range of irradiance levels (3-2250 μmol photons m^{-2} s^{-1}). A 1600-lumen dimmable soft white LED bulb was placed directly above the inline filter of the FeLume, and the brightness of the bulb was controlled manually with a dimmer switch. Photon flux and temperature were monitored using a spherical micro quantum photosynthetically active radiation (PAR) sensor (Walz) placed directly at the surface of the inline filter. Each of eight irradiance levels was maintained for about three minutes to allow chemiluminescence signals to stabilize, resulting in total scan times of ~30min per analysis. Temperature was recorded at least every 60s of this run time. Across all irradiance levels and replicate experiments, the temperature was 21.1(±0.3)°C (avg±std. dev), reflecting a low degree of variability (less than 1.6% coefficient of variation), which rules out any temperature effects on extracellular superoxide production by *T. oceanica*.

B_{Inst} increased substantially with each increase in irradiance, suggesting light-stimulated generation of superoxide in the absence of cells. To correct for this abiotic superoxide production in biological experiments, the amount of superoxide produced abiotically at each irradiance level ($[O_2^-]_{abio}$, pmol L^{-1}) was calculated as follows:

$$[O_2^-]_{abio} = \frac{(B_{Inst} - B_{SOD})}{S} \quad (5)$$

The average $[O_2^-]_{abio}$ at each light level ($[O_2^-]_{abio}^{AVG}$) was determined from three replicate scans. The superoxide produced by *T. oceanica* at each irradiance level was then calculated as:

$$[O_2^-]_{cells} = \frac{(L_{cells} - B_{cells+SOD})}{S} - [O_2^-]_{abio}^{AVG} \quad (6)$$

Finally, net rates of extracellular superoxide production at each irradiance level were calculated according to equation 4.

Net rates of extracellular superoxide production ($P^{O_2^-}$) and irradiance (E) data were fit to a double exponential equation modified from the photosynthesis-irradiance model of Platt et al.(30) by minimizing the sum of squared residuals using the Solver tool in Microsoft Excel:

$$P^{O_2^-} = P_D^{O_2^-} + P_S^{O_2^-}\left[1 - e^{\frac{-\alpha}{P_S^{O_2^-}}E}\right] e^{\frac{-\beta}{P_S^{O_2^-}}E} \quad (7)$$

where the fitted parameters included α, the initial linear slope of the best fit curve; β, the parameter describing the decrease of superoxide production rates at high irradiances; $P_D^{O_2^-}$, the net production rate of extracellular superoxide in the dark; and $P_S^{O_2^-}$, an estimate of the light-saturated rate of net extracellular superoxide production if β=0. Light-saturated rates of net extracellular superoxide production ($P_M^{O_2^-}$) and the minimum saturating irradiance of net extracellular superoxide production ($E_k^{O_2^-}$) were calculated by the following equations:

$$P_M^{O_2^-} = P_S^{O_2^-}\left(\frac{\alpha}{\alpha+\beta}\right)\left(\frac{\beta}{\alpha+\beta}\right)^{\beta/\alpha} + P_D^{O_2^-} \quad (8)$$

$$E_k^{O_2^-} = \frac{P_M^{O_2^-}}{\alpha} \quad (9)$$

Photophysiology measurements

T. oceanica cultures were sampled in mid-log phase and diluted with freshly filtered (0.22 µm) natural seawater to a final concentration of 10^6 cells mL^{-1}. Samples were amended with superoxide inhibitors at a similar per-cell dose as in FeLume experiments, corresponding to the following final concentrations: SOD (800 U L^{-1}), GSSG (8µM), DMSO (0.4%), or DPI (2µM) dissolved in 0.4% DMSO. Amended samples and unamended controls were incubated for 30 minutes while being exposed to darkness (0 µmol photons m^{-2} s^{-1}), dim light (~10 µmol photons m^{-2} s^{-1}), or high light (~2250 µmol photons m^{-2} s^{-1}). Temperature and irradiance levels were monitored every 60 seconds using a spherical micro quantum PAR sensor (Walz) to confirm stability of these conditions over the incubation period. The quantum efficiency of

photochemistry in photosystem II (PSII) was determined in treated cells using a fluorescence induction and relaxation (FIRe) fluorometer (Satlantic). Briefly, cells were quickly transferred from whatever light level to which they had been acclimated, placed in the FIRe in the dark and then illuminated with a single turnover flash of saturating blue excitation for a duration of 80 μsec. The quantum efficiency of PSII was calculated as F_v/F_m by the FIRePro data analysis package according to the equation:

$$F_v/F_m = \frac{F_m - F_0}{F_m} \qquad (10)$$

where F_m and F_0 are the maximum and minimum chlorophyll-a fluorescence intensities measured during and preceding the single turnover flash, respectively. Negative F_v/F_m values can arise when $F_m<F_0$ due to damage to the photosynthetic apparatus.

Statistical analyses

All statistical analyses were performed in JMP Pro 13.0. The effects of light and different chemical inhibitors and stimulants on superoxide production by ScGR, *T. oceanica* proteins and intact cells were assessed using Tukey's honest significant difference (HSD) test, Dunnett's test, or Student's t-test, as indicated. The growth of *T. oceanica* in the presence and absence of SOD was examined using Tukey's HSD test.

Results and Discussion

Extracellular superoxide production in aging batch cultures of *T. oceanica*

At 5 days (mid-log), 13 days (stationary phase), and 26 days (late stationary phase), *T. oceanica* produced extracellular superoxide at net rates of 66±14 amol cell^{-1} hr^{-1} (avg±SD; n=15), 41±15 amol cell^{-1} hr^{-1} (n=22), and 36±22 amol cell^{-1} hr^{-1} (n=20), respectively (Fig. S1). Assuming that net rates represent 20% of gross production, as previously quantified in a single growth phase of *T. oceanica* (3), the current results agree well with prior rates of gross extracellular superoxide production by this species (3). Moreover, results revealed that extracellular superoxide production rates were highest in exponential growth phase ($p<0.05$, Tukey HSD). Superoxide production and degradation likely occur simultaneously at the cell surface, so in principle, this trend could be driven by an increase in superoxide decay (e.g., higher expression of cell surface SODs) and/or a decrease in gross superoxide production across the growth curve. It is unclear how *T. oceanica* regulates net extracellular superoxide production over the growth curve, but this species has the ability to degrade extracellular superoxide, most likely via SOD (3). However, declining rates of net extracellular superoxide production across the growth curves of representative members of the ubiquitous *Roseobacter* clade of marine bacteria are regulated by decreases in gross superoxide production, rather than increases in decay (31). The same possibility should therefore be considered for *T. oceanica*. Regardless of the mechanisms, the decline of net extracellular superoxide production with increasing culture age challenges the perception of superoxide as a stress-response molecule in *T. oceanica*, given the continual drawdown of nutrients and accumulation of stress that occurs over time in batch cultures.

ToGR1 and ToGR2 sequence analysis

ToGR1 and ToGR2 share 99.4% sequence similarity across the predicted structural region of the protein and 93.7% similarity overall. Most of the sequence divergence is evident in the N-terminal domains outside of the enzyme catalytic structural region (Fig. S6), suggesting that the isoforms differ primarily in terms of their regulation and/or localization. There are three point substitutions within the catalytic structural region of the enzymes: in the interface C-terminal extension (E626 in ToGR1 and D610 in ToGR2), at several positions away from the C-terminal side of the second FAD binding domain (I471 in ToGR1 and K455 in ToGR2), and in a non-annotated region of the sequences (D394 in ToGR1 and N378 in ToGR2), see Fig. S6. It is unclear what significance, if any, these point substitutions have on the catalysis or interface binding domain of either GR isoform.

The most similar structurally-validated proteins to ToGR1 and ToGR2 included several trypanothione reductases (TRs; Tables S2 and S3; Fig. S7), which are closely related to GRs but exhibit a substrate preference for trypanothione, the parasite analog of oxidized glutathione (32). The family of GR and TR enzymes also exhibit large differences at the substrate interface (33). ToGR1 and ToGR2 exhibit the greatest structural similarity with TRs and EcGR based on shared features within this region (e.g., intersubunit C-terminal extension, intersubunit beta sheets) and do not consistently possess features that would suggest a substrate preference for trypanothione (hydrophobic patch, negatively charged active site) (18) over GSSG (Fig. S6). For example, most of the key substrate-binding sites for GSSG appear to be conserved or exhibit a

conservative amino acid substitution in ToGR1 and ToGR2 (Table S5). Furthermore, ToGR1 and ToGR2 are the BLASTP top hits when the *T. oceanica* genome is queried using a number of reference GR sequences (Table S4), indicating that these sequences are the most likely candidates for GR in *T. oceanica*. Together, these results support the annotation of ToGR1 and ToGR2 as glutathione reductases.

Potential localization of *T. oceanica* GR

Application of the ProtComp (SoftBerry) protein localization prediction tool revealed that ToGR1 and ToGR2 have a significant probability of extracellular secretion, which was not the case for known intracellular GR's (Table S6). These results are consistent with our detection of *T. oceanica* GR in the culture exudates. The same protein localization analysis also revealed that ToGR1, ToGR2, and homologous GR's are likely multi-located across several cellular compartments, including the cytoplasm, chloroplast, and mitochondria (Table S6). Thus, it is difficult to assess ToGR localization based on sequence analysis alone, yet these results suggest that ToGR1 and ToGR2 are distinct from related GR's based on the likelihood of extracellular secretion.

Because the putative N-terminal TM domain is adjacent and not integral to the functional enzyme structure (Fig. S6), the *T. oceanica* GRs could possibly retain their catalytic potential if disassociated from it. With the N-terminal domains attached, ToGR1 (634 AA) and ToGR2 (618 AA) have a predicted molecular weight of ~140 kDa as homodimers, assuming an average molecular weight of 110 Da per amino acid. With the cleavage of the N-terminal TM domains, however, the predicted molecular weights are ~107 kDa (the N-terminal domain is 147AA in ToGR1 and 131AA in ToGR2 [Fig. S6]), which is consistent with the finding of catalytically active GR in the ~100 kDa fraction of the cell exudate (Figure 1B-D).

Extracellular superoxide production by *T. oceanica* cells in the presence of inhibitors and stimulants

The ability of GSSG to eliminate extracellular superoxide production by whole cells could not be explained by direct reaction between superoxide and GSSG or any GSH generated through GSSG reduction. For example, superoxide calibration curves were unaffected by GSSG (Fig. S10). Furthermore, MCLA autooxidation generates a small amount of superoxide (34), which is eliminated by SOD (region (i) vs. (v) in Figure 2B). However, unlike SOD, GSSG did not eliminate the superoxide present in the instrument blank (region (i) ≈ (iv) > (v) in Figure 2B), which would not be the case if GSSG or GSH had degraded superoxide directly. These results therefore confirm that the inhibitory action of GSSG occurs via interaction with a putative cell surface protein, such as GR.

Exogenous NADPH did not stimulate extracellular superoxide production by whole cells (Figure 2A), in contrast to the stimulatory effect in protein extracts (Figure 1A). This result suggests that the NADPH-binding site of the superoxide-generating cell surface enzyme may not be accessible to extracellular NADPH. A number of possible reasons could be responsible for this finding, such as the orientation of the electron donor and electron acceptor binding sites of *T. oceanica* GR on opposite sides of the plasma membrane. This orientation is observed in Nox enzymes,

which couple the oxidation of cytosolic NADPH to the direct production of extracellular superoxide outside of the cell (5). Similar to results from *T. oceanica*, *Vibrio cholerae* generates extracellular superoxide by an inner membrane NADH dehydrogenase that couples the oxidation of cytosolic NADH on one side of the membrane to superoxide production on the opposite (periplasmic) side *(35)*. Exogenous additions of NADH did not stimulate extracellular superoxide production by *V. cholerae* due to the inability of NADH to cross the bacterial inner membrane *(35)*. In this case, superoxide is generated in the periplasm and could potentially exit the cell via pores in the outer membrane (36, 37). For *T. oceanica*, it is possible that GR might generate superoxide directly outside the cell, like Nox, and/or as in *V. cholerae*, there may be pores in the silica cell wall that potentially assist with the export of superoxide into the environment. In any case, the inability of exogenous NADPH to stimulate extracellular superoxide production by *T. oceanica* is consistent with the essential involvement of the cytosolic NADPH pool in this metabolism, consistent with transplasma membrane electron transport.

The effect of SOD on *T. oceanica* cultures

To test the potential function of extracellular superoxide generated by *T. oceanica*, cultures were grown in the presence of the antioxidant enzyme superoxide dismutase (SOD). SOD selectively degrades superoxide, and as a ~33 kDa protein, it is incapable of passively crossing biological membranes. Thus, SOD amendments specifically targeted the pool of superoxide in the extracellular environment. With daily additions of SOD, growth rates were ~6% faster and final cell yields were ~50% higher than controls that received daily additions of deionized water ($p<0.05$; Tukey HSD) (Fig. S11). These results could not be accounted for by additions of the diafiltered low molecular weight fraction (<10 kDa) of the SOD enzyme suspension, indicating that these responses were specifically due to SOD. The dismutation of superoxide by SOD generates hydrogen peroxide, which can diffuse back across the membrane into the cell, so the growth-stimulating effect of SOD amendments is probably not due to the removal of superoxide as a source of potentially harmful hydrogen peroxide. Rather, the positive effects of SOD on the growth of *T. oceanica* might be related to the direct detoxification of extracellular superoxide itself. For example, superoxide can react deleteriously with specific chemical functional groups and protein moieties, such as polyunsaturated fatty acids (38) and iron-sulfur clusters (36), causing damage to vital biomolecules and the potential build-up of toxic byproducts.

Alternative electron transport in phytoplankton

Similar to extracellular superoxide production, a number of alternative photosynthetic electron sinks involve the partial or complete reduction of oxygen. For example, in the chloroplast, the Mehler reaction circumvents $NADP^+$ reduction by generating superoxide, flavodiiron proteins couple oxygen reduction to the oxidation of photosynthetic NADPH, while the plastoquinone terminal oxidase (PTOX) diverts electron flow from $NADP^+$ to oxygen (39). In contrast to these mechanisms that occur intrinsically within chloroplasts, however, extracellular superoxide production requires the export of photosynthetic reducing power from its site of production. Excess reducing equivalents are in fact exported from chloroplasts through mechanisms that do not involve superoxide production, such as the malate valve and triosephosphate/3-phosphoglyceric acid shuttle. In a manner analogous to the proposed role of NADPH-dependent

514 extracellular superoxide production, these exported reducing equivalents are subsequently re-
515 oxidized in other cellular compartments, such as the cytosol and mitochondria, thereby providing
516 additional mechanisms to achieve cellular redox balance (39, 40).

517 **Table S1. BLASTP results for putative Nox homologs in the *T. oceanica* genome.** Only hits with E-values less than 10^{-5} are
518 reported.

Nox Sequence Query			Results from *T. oceanica* TaxID: 159749					
Species	**Name**	**Accession**	**Hit**	**Score**	**E value**	**Query cover (%)**	**Identity (%)**	**Genbank Accession**
Chlamydomonas reinhardtii	Rbo1	XP_001691855.1	hypothetical protein THAOC_13522	153	1.E-39	82	31	EJK65598.1
Chlamydomonas reinhardtii	Rbo2	XP_001691856.1	hypothetical protein THAOC_13522	157	6.E-41	87	28	EJK65598.1
			hypothetical protein THAOC_24795	58.9	7.E-09	40	25	EJK55472.1
			hypothetical protein THAOC_20318	56.6	3.E-08	40	24	EJK59461.1
Chondrus crispus	Rbo	AAZ73480	hypothetical protein THAOC_13522	95.9	2.E-20	27	32	EJK65598.1
			hypothetical protein THAOC_20318	54.7	2.E-07	30	25	EJK59461.1
			hypothetical protein THAOC_24795	53.1	7.E-07	30	26	EJK55472.1
Homo sapiens	Duox2	AAF78954	hypothetical protein THAOC_13522	105	5.E-23	21	23	EJK65598.1
			hypothetical protein THAOC_24795	62	2.E-09	23	24	EJK55472.1
			hypothetical protein THAOC_20318	58.5	3.E-08	23	22	EJK59461.1
			hypothetical protein THAOC_06435	52	3.E-06	21	22	EJK72071.1
Homo sapiens	Nox3	AAG17121	hypothetical protein THAOC_13522	81.3	5.E-16	47	23	EJK65598.1
			hypothetical protein THAOC_06435	57.8	1.E-08	24	26	EJK72071.1
			hypothetical protein THAOC_24795	52.4	6.E-07	30	25	EJK55472.1
			hypothetical protein THAOC_29999, partial	50.4	1.E-06	27	24	EJK50888.1
			hypothetical protein THAOC_20318	50.8	2.E-06	34	25	EJK59461.1
Arabidopsis thaliana	RboB	AAC39476	hypothetical protein THAOC_13522	87.4	1.E-17	35	25	EJK65598.1
			hypothetical protein THAOC_24795	54.7	2.E-07	30	23	EJK55472.1
			hypothetical protein THAOC_20318	52.8	7.E-07	33	23	EJK59461.1
			hypothetical protein THAOC_06435	48.9	1.E-05	26	22	EJK72071.1

519

Table S2: BLASTP results for the most similar sequences to ToGR1 in the UniProtKB and Protein Data Bank (PDB) databases. Trypanothione is the parasite analog of glutathione.

Top 5 hits overall (UniProtKB)				
Hit	**Score**	**E value**	**Identity (%)**	**UniProt Accession**
ToGR2 (*Thalassiosira oceanica*)	2924	0.0	93.7	K0TCW0
Glutathione reductase (*Thalassiosira pseudonana*)	2062	0.0	77.5	B8CEG9
Trypanothione reductase (*Fragilariopsis cylindrus*)	1799	0.0	72.5	A0A1E7EVV7
Trypanothione reductase (*Hondaea fermentalgiana*)	1335	3.7E-176	55.4	A0A2R5G4T6
Glutathione reductase (*Guillardia theta*)	1238	6.5E-162	51.2	L2JRB5
Top hits with 3D structural data (PDB)				
Hit	**Score**	**E value**	**Identity (%)**	**UniProt Accession**
Trypanothione reductase (*Trypanosoma brucei brucei*)	1022	2.4E-132	44.3	P39051
Trypanothione reductase (*Trypanosoma cruzi*)	1011	1.1E-130	43.6	P28593
Trypanothione reductase (*Crithidia fasciculata*)	970	1.4E-124	42.7	P39040
Glutathione reductase (*Eschericia coli*)	839	1.5E-105	41.8	P06715
Glutathione amide reductase (*Marichromatium gracile*)	782	6.4E-97	38.1	D0VWY5
Glutathione reductase (*Sacharromyces cerevisiae*)	769	9.6E-95	36.7	P41921
Glutathione reductase isoform 2 (*Sacharromyces cerevisiae*)	765	2.4E-94	37.4	P41921-2
Glutathione reductase (*Homo sapiens*)	742	2.8E-90	36.9	P00390

Table S3: BLASTP results for the most similar sequences to ToGR2 in the UniProtKB and Protein Data Bank (PDB) databases. Trypanothione is the parasite analog of glutathione.

Top 5 hits overall (UniProtKB)				
Hit	**Score**	**E value**	**Identity (%)**	**UniProt Accession**
ToGR1 (*Thalassiosira oceanica*)	2924	0.0	93.7	K0R3G6
Glutathione reductase (*Thalassiosira pseudonana*)	2054	0.0	77.3	B8CEG9
Trypanothione reductase (*Fragilariopsis cylindrus*)	1797	0.0	72.5	A0A1E7EVV7
Trypanothione reductase (*Hondaea fermentalgiana*)	1333	4.2E-176	55.4	A0A2R5G4T6
Glutathione reductase (*Guillardia theta*)	1236	7.6E-162	51.2	L2JRB5
Top hits with 3D structural data (PDB)				
Hit	**Score**	**E value**	**Identity (%)**	**UniProt Accession**
Trypanothione reductase (*Trypanosoma brucei brucei*)	1023	1.0E-132	44.5	P39051
Trypanothione reductase (*Trypanosoma cruzi*)	1011	6.6E-131	43.8	P28593
Trypanothione reductase (*Crithidia fasciculata*)	974	2.2E-125	43.1	P39040
Glutathione reductase (*Eschericia coli*)	834	5.2E-105	41.8	P06715
Glutathione amide reductase (*Marichromatium gracile*)	784	2.1E-97	38.1	D0VWY5
Glutathione reductase (*Sacharromyces cerevisiae*)	760	1.3E-93	36.7	P41921
Glutathione reductase isoform 2 (*Sacharromyces cerevisiae*)	756	3.3E-93	37.4	P41921-2
Glutathione reductase (*Homo sapiens*)	742	1.8E-90	36.9	P00390

Table S4. BLASTP results for putative glutathione reductases in the *T. oceanica* genome. Query sequences were from Hs=*Homo sapiens*, Sc=*Saccharomyces cerevisiae*, Ec=*Escherichia coli*, and Tc=*Trypanosoma cruzi*. GR=glutathione reductase, TR=trypanothione reductase. Accession numbers for ToGR1 and ToGR2 are EJK45974 and EJK71311, respectively, which are the top hits in every search.

Query	NCBI accession	% ID	Alignment length	Query start	Query end	Subject start	Subject end	E-value	Bit score
HsGR	EJK71311.1	37.284	464	35	478	149	594	9.02E-86	275
HsGR	EJK45974.1	37.284	464	35	478	165	610	3.22E-85	274
HsGR	EJK50234.1	27.5	480	7	474	30	499	1.33E-39	149
HsGR	EJK73038.1	27.565	497	4	474	223	703	3.85E-39	150
HsGR	EJK64319.1	27.941	476	21	474	207	649	8.75E-38	146
HsGR	EJK58680.1	29.095	409	4	382	121	511	1.75E-34	135
HsGR	EJK53151.1	29.023	348	21	331	81	418	1.16E-26	113
HsGR	EJK66633.1	75	36	443	478	1	36	2.62E-13	64.3
HsGR	EJK53821.1	20.235	425	32	392	21	429	2.16E-09	59.3
HsGR	EJK68310.1	21.932	497	21	445	74	545	1.02E-06	51.2
HsGR	EJK51497.1	42.857	42	24	64	122	163	3.7	30
HsGR	EJK43713.1	29.577	71	152	222	10	78	4.7	28.9
HsGR	EJK62072.1	50	28	21	48	17	44	8.3	28.9
ScGR	EJK71311.1	35.745	470	26	478	149	601	3.32E-86	276
ScGR	EJK45974.1	35.774	478	26	478	165	617	3.32E-87	279
ScGR	EJK50234.1	26.386	451	26	465	60	497	1.33E-35	138
ScGR	EJK73038.1	24.544	493	12	467	231	703	1.54E-33	134
ScGR	EJK64319.1	25.62	484	9	477	204	659	1.26E-31	128
ScGR	EJK58680.1	26.895	409	12	383	129	519	1.76E-30	124
ScGR	EJK53151.1	25.291	344	12	327	81	423	3.73E-26	111
ScGR	EJK66633.1	62.791	43	436	478	1	43	4.31E-14	66.6
ScGR	EJK53821.1	22.066	426	23	386	21	430	6.62E-14	73.6
ScGR	EJK51497.1	33.871	62	5	65	112	172	2.7	30.4
EcGR	EJK71311.1	41.518	448	23	450	153	594	8.83E-98	305
EcGR	EJK45974.1	41.518	448	23	450	169	610	3.75E-98	307
EcGR	EJK50234.1	26.244	442	22	446	63	499	1.30E-36	140
EcGR	EJK73038.1	27.01	485	5	444	231	701	7.37E-36	140
EcGR	EJK64319.1	28.228	457	2	441	204	644	6.46E-31	125
EcGR	EJK58680.1	29.351	385	5	354	129	511	4.36E-34	133
EcGR	EJK53151.1	28.655	342	5	303	81	418	5.54E-26	110
EcGR	EJK66633.1	75	36	415	450	1	36	2.06E-13	64.7
EcGR	EJK53821.1	21.636	379	38	365	53	430	6.31E-10	60.8
TcTR	EJK71311.1	43.764	457	29	483	159	607	1.20E-126	381
TcTR	EJK45974.1	43.545	457	29	483	175	623	5.66E-126	380
TcTR	EJK50234.1	27.211	441	47	467	80	503	2.50E-33	132
TcTR	EJK73038.1	22.524	515	4	466	231	703	1.96E-17	85.1
TcTR	EJK64319.1	23.447	499	3	484	206	663	4.95E-21	96.3
TcTR	EJK58680.1	23.153	406	4	375	129	511	5.27E-16	80.1
TcTR	EJK53151.1	24.862	362	3	330	80	423	3.53E-15	77.8
TcTR	EJK66633.1	63.265	49	435	483	1	49	5.38E-16	72
TcTR	EJK53821.1	22.437	517	15	461	21	510	4.89E-07	52
TcTR	EJK68310.1	29.358	327	155	456	245	564	8.56E-19	89.4

Table S5: Comparison of substrate binding sites of ToGR1 and ToGR2 to reference flavoprotein disulfide reductases. To=*Thalassiosira oceanica*, Hs=*Homo sapiens,* Sc=*Saccharomyces cerevisiae,* Ec=*Escherichia coli,*, Tc=*Trypanosoma cruzi,* GR=glutathione reductase, TR=trypanothione reductase. The sequence positions are provided for ToGR1 and ToGR2.

Amino acid properties
hydrophobic
polar
positive
negative
uncharged
aromatic

Sequence	Substrate binding site (see Supplementary Figure 6)				
	1	2	3	4	5
ToGR1	R164	R167	V154	V158	H482
ToGR2	R148	R151	V238	V242	H466
HsGR	A	R	I	N	R
ScGR	A	R	I	N	R
EcGR	A	N	S	V	R
TcTR	E	W	S	M	A
	↓	↓	↓	↓	↓
Closest similarity	no conservation	GR	GR	inconclusive	GR

Table S6: Predicted localization of ToGR1 and ToGR2 compared to reference glutathione reductases. Reference GRs are from *Homo sapiens* (HsGR), *Saccharomyces cerevisiae* (ScGR), and *Escherichia coli* (EcGR). Analysis was performed with ProtComp by Softberry (www.softberry.com). ProtComp utilizes several methods, including neural networks-based analysis, to predict protein localization across each of 4 to 10 cellular compartments and combines these results into an integrated final score. For brevity, only results from the neural networks and integrated analyses are shown here. ProtComp also conducts structure-based BLAST (SBLAST) of query sequences against a database of multilocated proteins, and if significant similarity is found, the predicted multilocalizations are reported. Neural networks analysis predicted that ToGR1 and ToGR2 have a probability of extracellular secretion but that the reference GR's do not. Simultenously, the integrated scores and SBLAST analysis support localization of the *T. oceanica* GR's across multiple cellular compartments (see SI Appendix, Results and Discussion). n/a = not applicable

Prediction Method	Cell compartment	Score				
		ToGR1	ToGR2	HsGR	ScGR	EcGR
Neural Networks	Nuclear	0.00	0.00	0.04	0.18	n/a
	Plasma membrane	0.91	0.91	0.07	0.09	0.06
	Extracellular	0.91	0.91	0.00	0.00	0.00
	Cytoplasmic	0.00	0.00	2.62	3.74	2.94
	Mitochondrial	0.00	0.00	0.51	0.00	n/a
	Endoplas. Ret.	0.00	0.00	0.03	0.03	n/a
	Peroxisomal	0.91	0.91	0.75	0.00	n/a
	Lysosomal	n/a	n/a	0.00	0.00	n/a
	Golgi	0.27	0.27	0.00	0.02	n/a
	Chloroplast	1.50	0.00	n/a	n/a	n/a
	Vacuolar	0.00	0.00	0.00	0.00	n/a
	Periplasmic	n/a	n/a	n/a	n/a	0.00
	Overall prediction	Extracellular (secreted)	Extracellular (secreted)	Cytoplasmic	Cytoplasmic	Cytoplasmic
Integrated	Nuclear	0.02	0.02	0.00	0.00	n/a
	Plasma membrane	0.03	0.04	0.00	0.00	1.88
	Extracellular	0.00	0.00	0.01	0.00	0.00
	Cytoplasmic	7.85	4.98	6.47	6.74	8.12
	Mitochondrial	0.02	2.83	3.52	3.24	n/a
	Endoplas. Ret.	0.05	0.13	0.00	0.02	n/a
	Peroxisomal	0.00	0.00	0.00	0.00	n/a
	Lysosomal	n/a	n/a	0.00	0.00	n/a
	Golgi	0.00	0.00	0.00	0.00	n/a
	Chloroplast	1.77	1.72	n/a	n/a	n/a
	Vacuolar	0.27	0.27	0.00	0.00	n/a
	Periplasmic	n/a	n/a	n/a	n/a	0.00
	Overall prediction	Cytoplasmic	Cytoplasmic	Cytoplasmic	Cytoplasmic	Cytoplasmic
SBLAST	Overall Prediction	Multilocated to chloroplast, mitochondria	Multilocated to chloroplast, mitochondria	Multilocated to cytoplasm, nucleus, and endoplasmic reticulum	Multilocated to cytoplasm, nucleus, and endoplasmic reticulum	No multilocation reported

Table S7: Signal peptides predicted by PrediSi. Sequences were analyzed using default parameters after selecting the appropriate organism group (www.predisi.de) ref. (23). To=*Thalassiosira oceanica*, Hs=*Homo sapiens*, Ec=*Escherichia coli*, Sc=*Saccharomyces cerevisiae*, Tc=*Trypanosoma cruzi*, GR=glutathione reductase, TR=trypanothione reductase.

Protein	Sequence Database	Accession	PrediSi		
			Signal peptide?	Score	Cleavage position
ToGR1	NCBI	EJK45974	No	0.4334	61
ToGR2	NCBI	EJK71311	Yes	0.6052	57
HsGR	PDB	3GRS	No	0.2191	39
EcGR	PDB	1GER	No	0.0000	23
ScGR	PDB	2HQM	No	0.1512	30
TcTR	PDB	1AOG	No	0.4063	18

Table S8: Transmembrane regions predicted by tmap. Sequences were analyzed using default parameters (http://www.bioinformatics.nl/cgi-bin/emboss/tmap) ref. (24). To=*Thalassiosira oceanica*, Hs=*Homo sapiens*, Ec=*Escherichia coli*, Sc=*Saccharomyces cerevisiae*, Tc=*Trypanosoma cruzi*, GR=glutathione reductase, TR=trypanothione reductase. The hits indicated with an asterisk (*) are likely erroneous because these sequences span the conserved NADPH binding site (Fig S6).

Protein	Sequence Database	Accession	tmap			
			Hit #	start	end	TM sequence
ToGR1	NCBI	EJK45974	1	Met98	Val116	MKVMSSLLLTAASAAAFQV
			2*	Ser332	Gly351	SMVVVGGGFIALEFATIMDG
ToGR2	NCBI	EJK71311	1	Ala33	Leu56	ARRKPARAYFFWLAGFLPSSPAFL
			2	Met82	Ala110	MKVMSSLLLTAASAAAFQVRPTAKTYLRA
			3*	Ser316	Gly335	SMVVVGGGFIALEFATIMDG
HsGR	PDB	3GRS	1*	Arg189	Ile217	RSVIVGAGYIAVEMAGILSALGSKTSLMI
EcGR	PDB	1GER	1*	Pro167	Leu189	PERVAVVGAGYIAVELAGVINGL
ScGR	PDB	2HQM	1*	Val189	Gly206	VVVGAGYIGIELAGVFHG
TcTR	PDB	1AOG	1*	Arg188	Asp213	RRVLTVGGGFISVEFAGIFNAYKPKD

Table S9: Superoxide-irradiance curve parameters. Net rates of extracellular superoxide production and irradiance data were fit to a double exponential equation modified from the photosynthesis-irradiance model of Platt et al.(30) using data from each biological replicate (a, b, c) or all biological replicates (see Methods).

Bio Rep	$P_D^{O_2^-}$	$P_S^{O_2^-}$	$P_M^{O_2^-}$	α	β	$E_k^{O_2^-}$	R^2
	amol cell^{-1} hr^{-1}			$\frac{\text{amol cell}^{-1}\ \text{hr}^{-1}}{\mu\text{mol m}^{-2}\ \text{s}^{-1}}$		μmol m^{-2} s^{-1}	
All	24.8	32.9	55.1	0.31	0.005	179.2	0.77
a	28.2	25.8	51.1	0.39	0.010	130.9	0.98
b	16.7	42.4	57.7	0.34	0.002	167.6	1.00
c	29.4	33.6	58.8	0.23	0.007	259.6	0.99

Table S10: BLASTP top hits for putative *T. oceanica* GR and Nox homologs in representative eukaryotic phytoplankton genomes. To=*Thalassiosira oceanica*, Cr= *Chlamydomonas reinhardtii*, Cc=*Chondrus crispus*, Hs=*Homo sapiens*, At=*Arabidopsis thaliana*

Genome	Query	Hit	Score	E Value	Query Cover (%)	Identity (%)	Accession Number
Thalassiosira pseudonana	ToGR	glutathione reductase, gro-2 [Thalassiosira pseudonana CCMP1335]	814	0	76	79	XP_002294541.1
	CrRbo1	ferric reductase-like protein [Thalassiosira pseudonana CCMP1335]	96.7	6.00E-22	55	26	XP_002288167.1
	CrRbo2	ferric reductase-like protein [Thalassiosira pseudonana CCMP1335]	91.3	4.00E-20	51	23	XP_002288167.1
	CcRbo	ferric reductase-like protein [Thalassiosira pseudonana CCMP1335]	70.1	6.00E-13	12	39	XP_002288167.1
	HsDuox2	ferric reductase-like protein [Thalassiosira pseudonana CCMP1335]	89.4	6.00E-19	28	22	XP_002288167.1
	HsNox3	ferric reductase-like transmembrane component [Thalassiosira pseudonana CCMP1335]	93.6	1.00E-20	67	24	XP_002286589.1
	AtRboB	ferric reductase-like protein [Thalassiosira pseudonana CCMP1335]	92.8	2.00E-20	36	26	XP_002288167.1
Phaeodactylum tricornutum	ToGR	glutathione reductase [Phaeodactylum tricornutum CCAP 1055/1]	358	8.00E-118	74	44	XP_002180322.1
	CrRbo1	ferric reductase [Phaeodactylum tricornutum CCAP 1055/1]	80.5	3.00E-16	21	37	XP_002183592.1
	CrRbo2	ferric reductase [Phaeodactylum tricornutum CCAP 1055/1]	87.8	2.00E-18	26	35	XP_002183592.1
	CcRbo	ferric reductase [Phaeodactylum tricornutum CCAP 1055/1]	173	1.00E-45	43	34	XP_002179812.1
	HsDuox2	ferric reductase [Phaeodactylum tricornutum CCAP 1055/1]	95.1	6.00E-20	22	27	XP_002179812.1
	HsNox3	ferric reductase [Phaeodactylum tricornutum CCAP 1055/1]	87.8	2.00E-18	86	25	XP_002179812.1
	AtRboB	ferric reductase [Phaeodactylum tricornutum CCAP 1055/1]	105	2.00E-23	48	26	XP_002183592.1
Fragilariopsis cylindricus	ToGR	Trypanothione reductase [Fragilariopsis cylindrus CCMP1102]	696	0.00E+00	72	72	OEU09673.1
	CrRbo1	ferric-chelate reductase [Fragilariopsis cylindrus CCMP1102]	70.5	8.00E-13	26	30	OEU22811.1
	CrRbo2	ferric-chelate reductase [Fragilariopsis cylindrus CCMP1102]	81.6	2.00E-16	34	30	OEU22811.1
	CcRbo	ferric-chelate reductase [Fragilariopsis cylindrus CCMP1102]	154	5.00E-39	46	29	OEU18178.1
	HsDuox2	ferric-chelate reductase [Fragilariopsis cylindrus CCMP1102]	114	2.00E-25	19	27	OEU22811.1
	HsNox3	ferric-chelate reductase [Fragilariopsis cylindrus CCMP1102]	79.7	1.00E-15	49	25	OEU22811.1
	AtRboB	putative ferric reductase [Fragilariopsis cylindrus CCMP1102]	114	5.00E-26	41	29	OEU12891.1
Emiliania huxleyi	ToGR	thioredoxin reductase [Emiliania huxleyi CCMP1516]	272	3.00E-84	72	37	XP_005756463.1
	CrRbo1	hypothetical protein EMIHUDRAFT_232597 [Emiliania huxleyi CCMP1516]	77.8	2.00E-16	25	36	XP_005783048.1
	CrRbo2	hypothetical protein EMIHUDRAFT_232597 [Emiliania huxleyi CCMP1516]	81.3	9.00E-18	25	38	XP_005783048.1
	CcRbo	hypothetical protein EMIHUDRAFT_215378 [Emiliania huxleyi CCMP1516]	111	1.00E-25	35	33	XP_005763064.1
	HsDuox2	hypothetical protein EMIHUDRAFT_416147 [Emiliania huxleyi CCMP1516]	146	5.00E-37	29	27	XP_005768827.1
	HsNox3	hypothetical protein EMIHUDRAFT_416147 [Emiliania huxleyi CCMP1516]	204	2.00E-59	89	30	XP_005768827.1
	AtRboB	hypothetical protein EMIHUDRAFT_416147 [Emiliania huxleyi CCMP1516]	175	2.00E-47	58	28	XP_005768827.1
Symbiodinium microadriaticum	ToGR	Glutathione reductase, chloroplastic [Symbiodinium microadriaticum]	348	3.00E-104	74	39	OLP89676.1
	CrRbo1	Superoxide-generating NADPH oxidase heavy chain subunit A [Symbiodinium microadriaticum]	177	7.00E-47	82	33	OLQ10272.1
	CrRbo2	Superoxide-generating NADPH oxidase heavy chain subunit A [Symbiodinium microadriaticum]	172	3.00E-45	90	32	OLQ10272.1
	CcRbo	Superoxide-generating NADPH oxidase heavy chain subunit A [Symbiodinium microadriaticum]	95.9	1.00E-19	29	26	OLQ10272.1
	HsDuox2	putative respiratory burst oxidase-like protein G [Symbiodinium microadriaticum]	154	4.00E-37	28	26	OLP85719.1
	HsNox3	putative respiratory burst oxidase-like protein G [Symbiodinium microadriaticum]	134	2.00E-32	90	23	OLP85719.1
	AtRboB	putative respiratory burst oxidase-like protein G [Symbiodinium microadriaticum]	191	1.00E-49	63	26	OLP85719.1
Ostreococcus tauri	ToGR	hypothetical protein BE221DRAFT_202020 [Ostreococcus tauri]	394	1.00E-131	73	47	OUS42079.1
	CrRbo1	No hit	n/a	n/a	n/a	n/a	n/a
	CrRbo2	hypothetical protein BE221DRAFT_67900 [Ostreococcus tauri]	29.3	4.5	5	48	OUS48792.1
	CcRbo	ferric reductase [Ostreococcus tauri]	78.6	2.00E-15	27	27	OUS48954.1
	HsDuox2	ferric reductase [Ostreococcus tauri]	79.7	2.00E-15	20	23	OUS48954.1
	HsNox3	ferric reductase [Ostreococcus tauri]	63.5	6.00E-11	46	25	OUS48954.1
	AtRboB	ferric reductase [Ostreococcus tauri]	63.9	1.00E-10	48	20	OUS48954.1
Micromonas pusilla	ToGR	predicted protein [Micromonas pusilla CCMP1545]	399	1.00E-133	72	47	XP_003060818.1
	CrRbo1	predicted protein [Micromonas pusilla CCMP1545]	58.5	3.00E-09	19	29	XP_003055885.1
	CrRbo2	predicted protein [Micromonas pusilla CCMP1545]	64.3	4.00E-11	23	31	XP_003055885.1
	CcRbo	predicted protein [Micromonas pusilla CCMP1545]	92.8	1.00E-19	14	40	XP_003055885.1
	HsDuox2	predicted protein [Micromonas pusilla CCMP1545]	61.2	2.00E-09	7	30	XP_003055885.1
	HsNox3	predicted protein [Micromonas pusilla CCMP1545]	73.6	6.00E-14	47	25	XP_003056236.1
	AtRboB	predicted protein [Micromonas pusilla CCMP1545]	77.8	6.00E-15	19	27	XP_003055885.1

Table S11: Sequence analysis of select *T. oceanica* GR homologs present in representative marine phytoplankton genomes. Representative phytoplankton genomes were searched via BLASTP analysis for putative homologs of *T. oceanica* GR using ToGR1 as the query sequence. Each putative homolog in the table below was also analyzed for the protein localization and presence of putative N-terminal transmembrane (TM) domains, signal peptides, and conserved catalytic domains. Consensus sequences for the catalytic domains were derived from structure-based multiple sequence alignment with ToGR1, ToGR2, and reference flavoprotein disulfide reductases, see Fig. S6. (t=tiny; @=aromatic; s=small; l=aliphatic).

Protein data	Species	*Thalassiosira pseudonana*	*Phaeodactylum tricornutum*	*Emiliania huxleyi*	*Ostreococcus tauri*	*Micromonas pusilla*
	NCBI accession	XP_002296642	XP_002181543	XP_005781728	OUS42553	XP_003060770
	Total AA length	498	630	500	848	565
ToGR1 BLASTP results	Score	172	237	226	245	166
	Query coverage	79%	72%	72%	75%	71%
	% Identity	29%	35%	36%	37%	30%
	E-value	3.00E-47	6.00E-70	2.00E-66	3.00E-71	9.00E-45
Protein localization	Probability of extracellular secretion (ProtComp)?	Yes	Yes	Yes	Yes	Yes
N-terminal TM or signal peptide	database	PrediSi	tmap	PrediSi/Polyphob.	Polyphobius	Polyphobius
	start	1	18	1	232	1
	end	17	39	21 or 23	253	15
	Notes	score = 0.5399	n/a	score=0.5838	n/a	n/a
First FAD binding site consensus: GtGSGG	start	G48	G143	G42	G365	G103
	end	G53	G148	G47	G370	G108
	sequence	GCGVGG	GGGSGG	GGGSGG	GGGSGG	GAGVGG
catalytic disulfide consensus: GGTCVNVGCVPKK	start	G76	G180	G82	G402	G131
	end	K88	K192	K94	K414	K143
	sequence	GGTCVNRGCVPSK	GGTCVNVGCIPKK	GGTCVNVGCVPKK	GGTCVNVGCIPKK	GGTCVNRGCVPSK
NADPH binding site consensus: VGtG@I	start	I221	V337	V215	V541	I268
	end	I227	I343	I221	V547	I374
	sequence	IGSGYI	VGASYI	VGAGYI	VGASYI	IGSGYI
second FAD binding site consensus: TNVXslYAlGD	start	not conserved	T456	T314	T665	not conserved
	end		D467	D325	D676	
	sequence		THCPNIYAIGD	TGVSGLYCLGD	TNVPNIYAIGD	

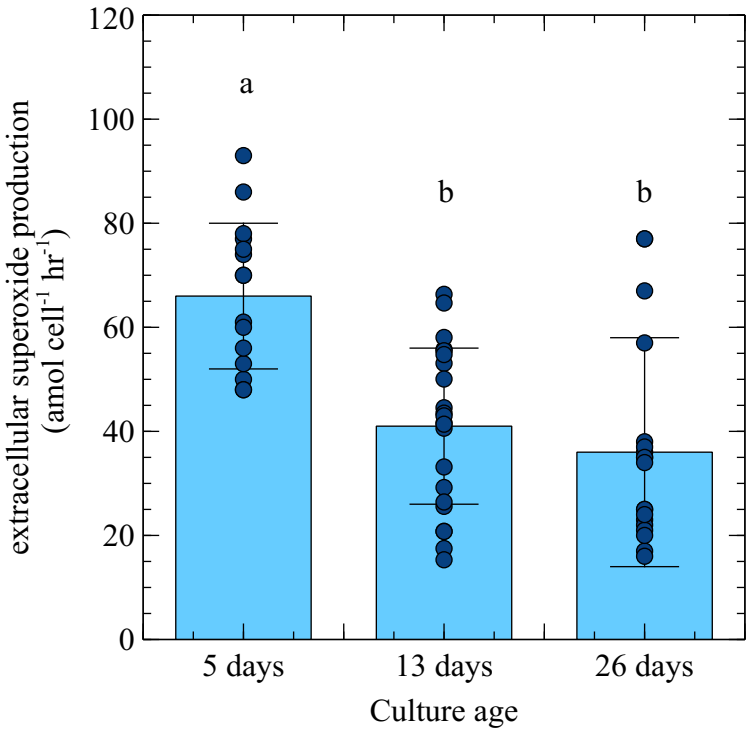

Fig. S1. Extracellular superoxide production by aging batch cultures of *T. oceanica*. Bars represent the average ± std. dev. of biological replicates (n=15, 22, and 20 at 5, 13, and 26 days, respectively). Individual points represent data from each biological replicate. Observations not connected by the same letter are significantly different (Tukey HSD, $p<0.05$).

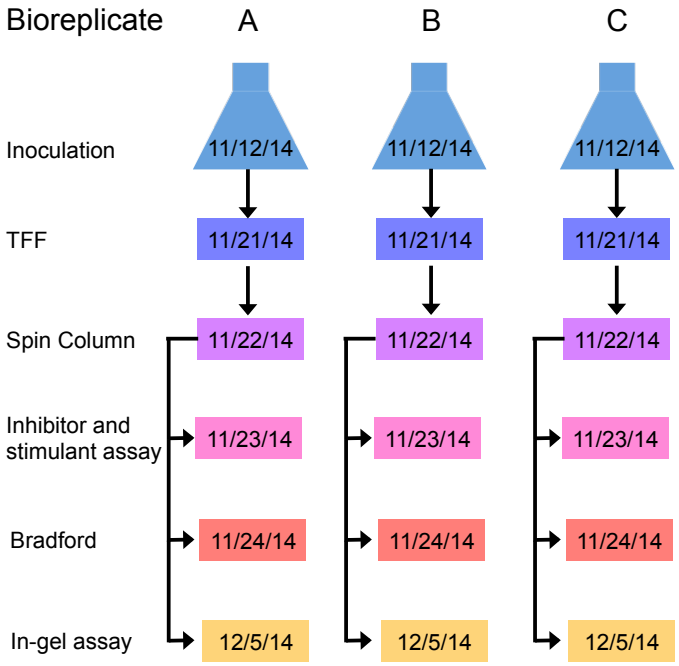

Fig. S2: Sampling overview of concentrated extracellular proteins used to assess the effect of inhibitors and stimulants on extracellular superoxide production

627

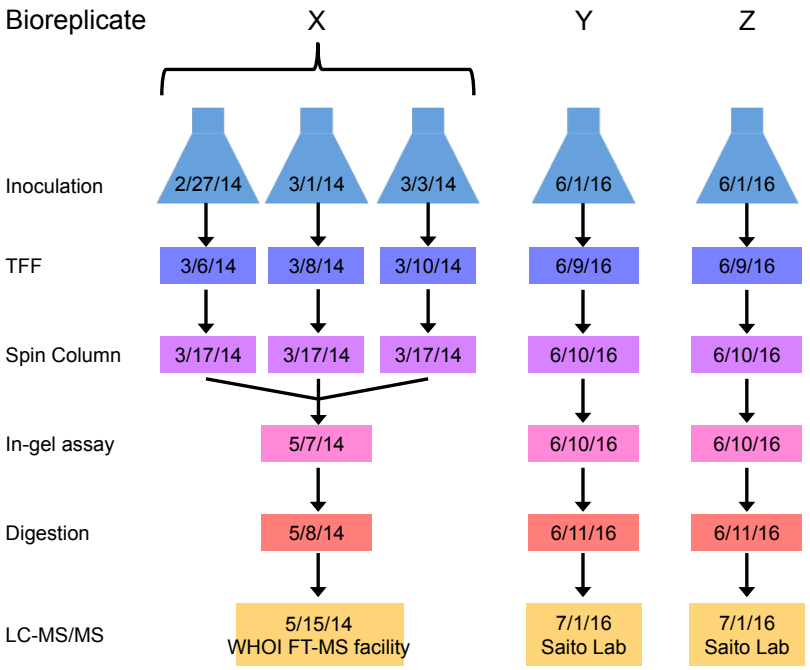

628
629
630
631 **Fig. S3: Sampling overview of concentrated extracellular proteins used for peptide**
632 **fingerprinting**

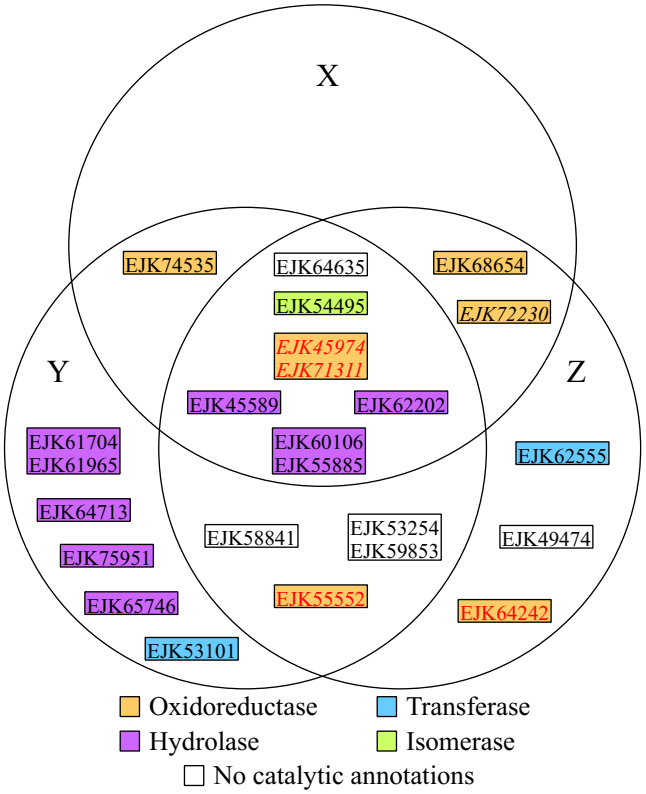

Fig. S4: Protein diversity and distribution in NBT bands revealed by LC/MS/MS peptide fingerprinting. X, Y, and Z are biological replicates. Each protein is represented by its NCBI accession number. Highly similar protein sequences sharing one or more unique peptides are depicted in the same box. The text format indicates whether the protein sequence contains a putative NADPH binding site (italic) or a predicted flavin binding site (red). Full results are presented in Dataset S1.

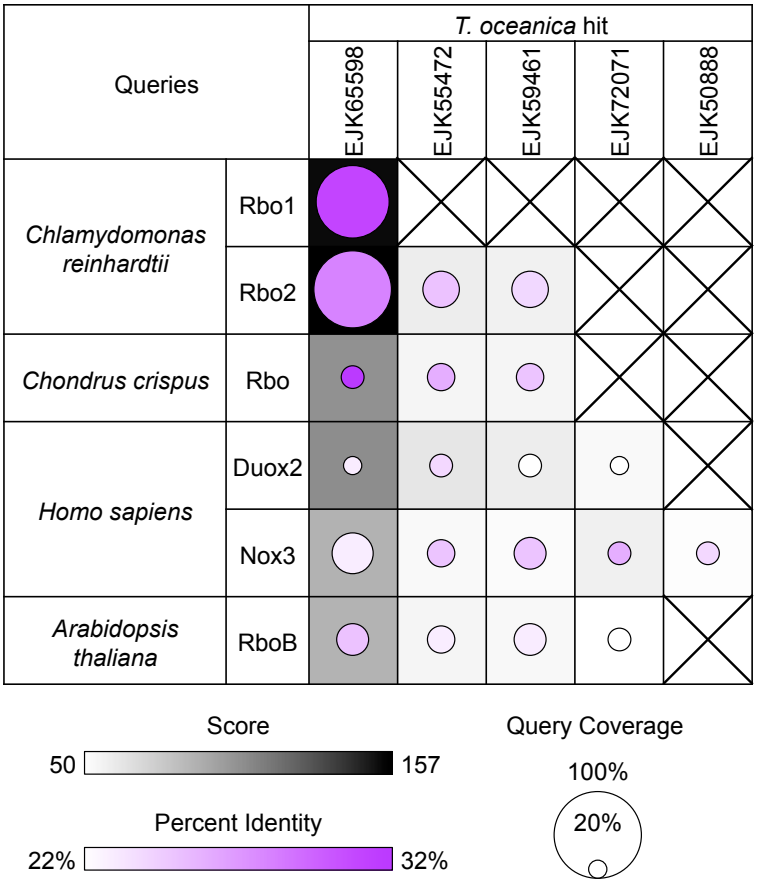

Fig. S5: Putative homologs of NADPH oxidases in the *T. oceanica* genome. BLASTP query sequences included canonical NADPH oxidase (Nox), Dual oxidase (Duox), and respiratory burst oxidases (Rbo) from human, the flowering plant *A. thaliana*, and algae. Full results are presented in Table S1. Only hits with E-values less than 10^{-5} are reported.

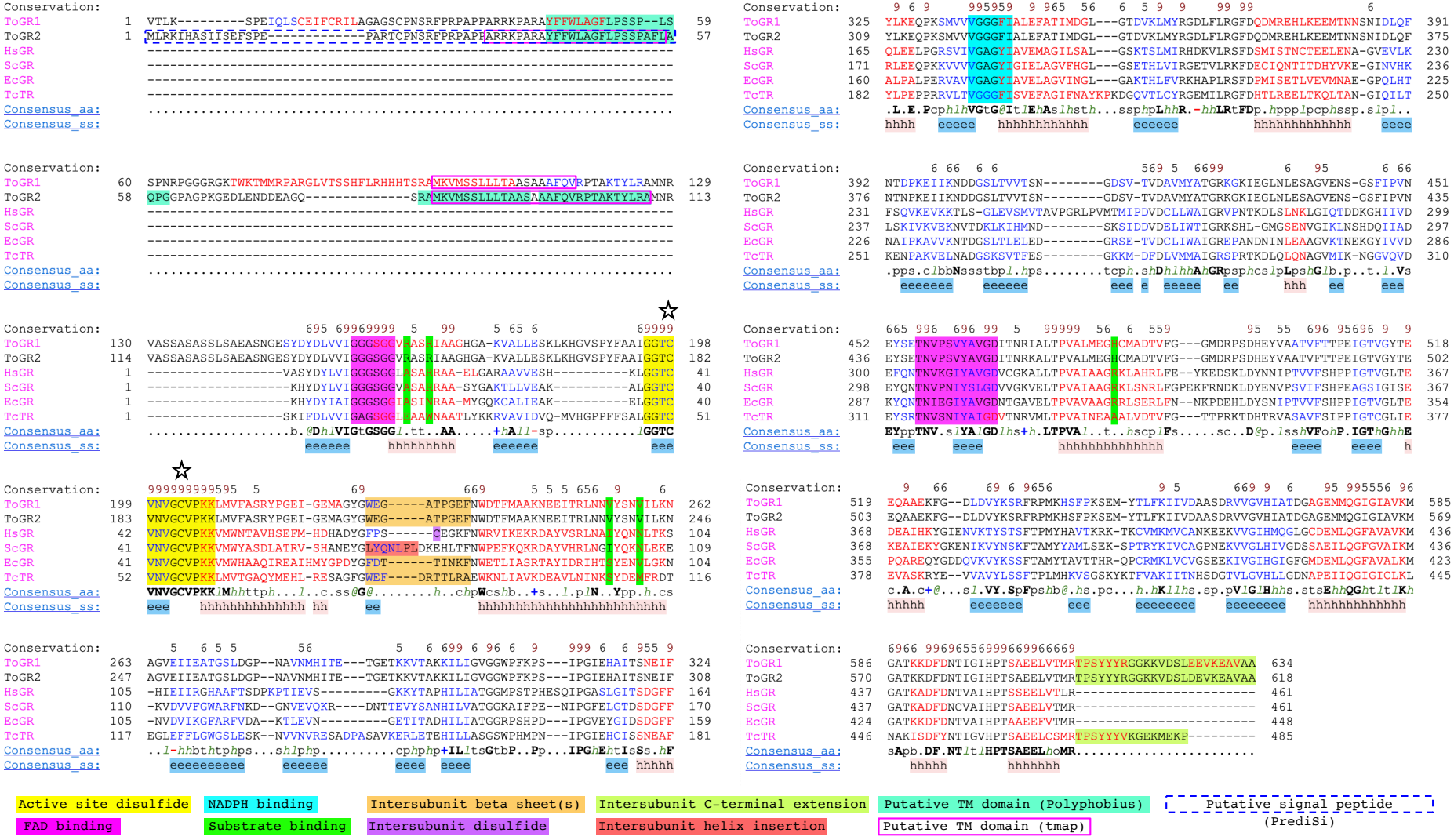

Fig. S6: Structure-based multiple sequence alignment of ToGR1 and ToGR2 to reference flavoprotein disulfide reductases. Reference proteins are glutathione reductase from *Homo sapiens* (HsGR), *Escherichia coli* (EcGR), and *Saccharomyces cerevisiae* (ScGR), and trypanothione reductase from *Trypanosoma cruzi* (TcTR). The first line in each block shows conservation indices for positions with a conservation index above 4. The last two lines show consensus amino acid sequence (Consensus_aa) and consensus predicted secondary structures (Consensus_ss). Representative sequences have magenta names and they are colored according to predicted secondary structures (red: alpha-helix, blue: beta-strand). The sequences with black names directly under a representative sequence are in the same pre-aligned group and are aligned in a fast way. Consensus predicted secondary structure symbols: alpha-helix: h; beta-strand: e. Consensus amino acid symbols are: conserved amino acids are in bold and uppercase letters; aliphatic (I, V, L): *l*; aromatic (Y, H, W, F): *@*; hydrophobic (W, F, Y, M, L, I, V, A, C, T, H): *h*; alcohol (S, T): o; polar residues (D, E, H, K, N, Q, R, S, T): p; tiny (A, G, C, S): t; small (A, G, C, S, V, N, D, T, P): s; bulky residues (E, F, I, K, L, M, Q, R, W, Y): b; positively charged (K, R, H): +; negatively charged (D, E): -; charged (D, E, K, R, H): c. Note that for some reference sequences, especially HsGR, the alignment excludes some terminal amino acids that are not present in the protein structure, which alters the numbered position of amino acids in the figure above relative to the full protein sequence. Stars indicate the two Cys residues that form the catalytic disulfide.

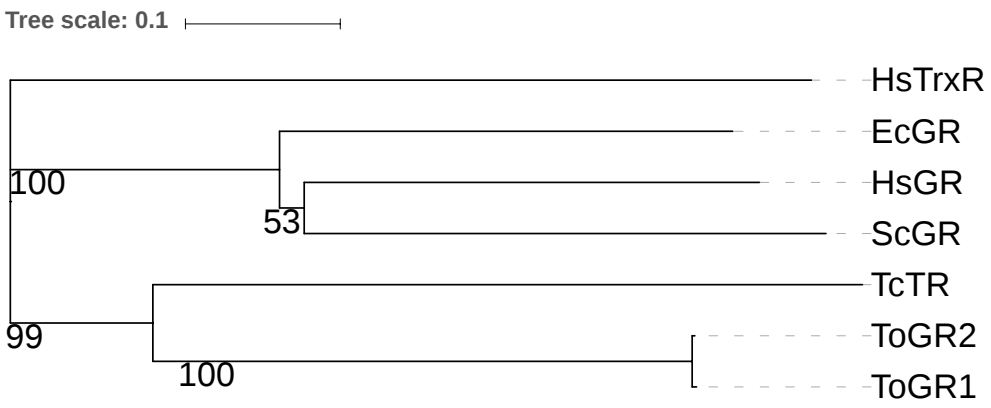

Fig. S7: Phylogenetic tree of ToGR1, ToGR2, and related flavoprotein disulfide reductases. The scale bar indicates a relative measure of the distance in the tree. Bootstrap values are shown. Hs = *Homo sapiens*, Ec = *Escherichia coli*, Sc = *Saccharomyces cerevisiae*, Tc = *Trypanosoma cruzi*, To = *Thalassiosira oceanica*. TrxR = thioredoxin reductase, GR = glutathione reductase, TR = trypanothione reductase. HsTrxR is provided as an outgroup.

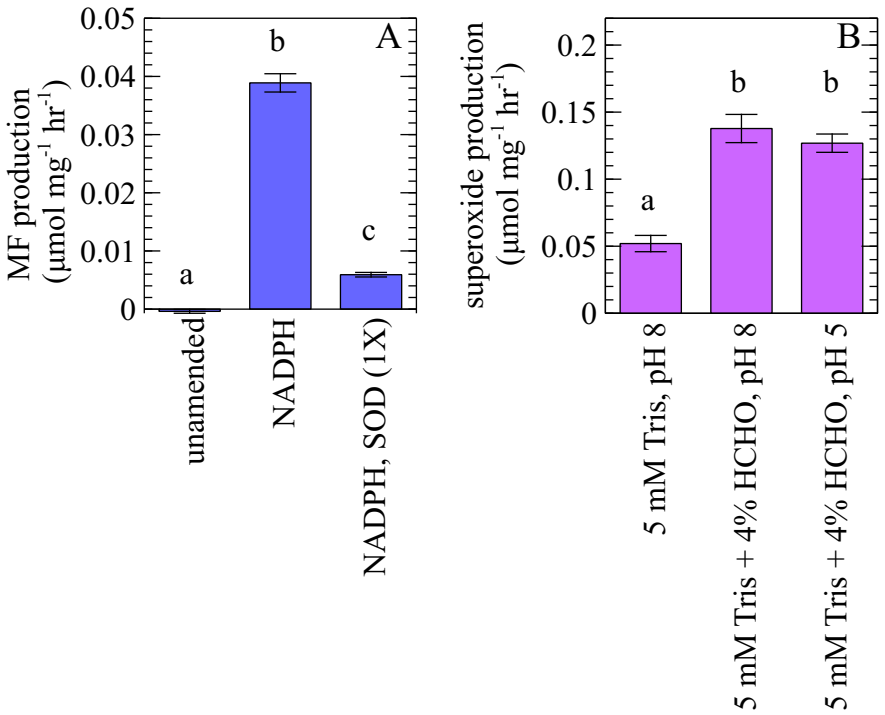

Fig. S8: NADPH-dependent superoxide production by *Saccharomyces cerevisiae* glutathione reductase (ScGR). (A) NBT reduction to monoformazan (MF) by ScGR in the presence of NADPH. SOD treatments show some superoxide-independent NBT reduction. Superoxide production is therefore represented after accounting for SOD controls and applying the MF:superoxide reaction stoichiometry (1:2) ref. (2). (B) The effect of formaldehyde on NADPH-dependent superoxide production by ScGR. Formaldehyde (HCHO) was added to ScGR enzyme suspensions at a final concentration of 4% at different pH and then removed via diafiltration. The pretreated enzymes were then screened for superoxide production in the presence of NADPH without the addition of formaldehyde. Rates of superoxide production were calculated by subtracting rates of MF production in the presence of NADPH and SOD. In both panels, data represent the average ± std. dev. of 3 biological replicates. Treatments not connected by the same letter are significantly different (Tukey HSD, $p<0.05$).

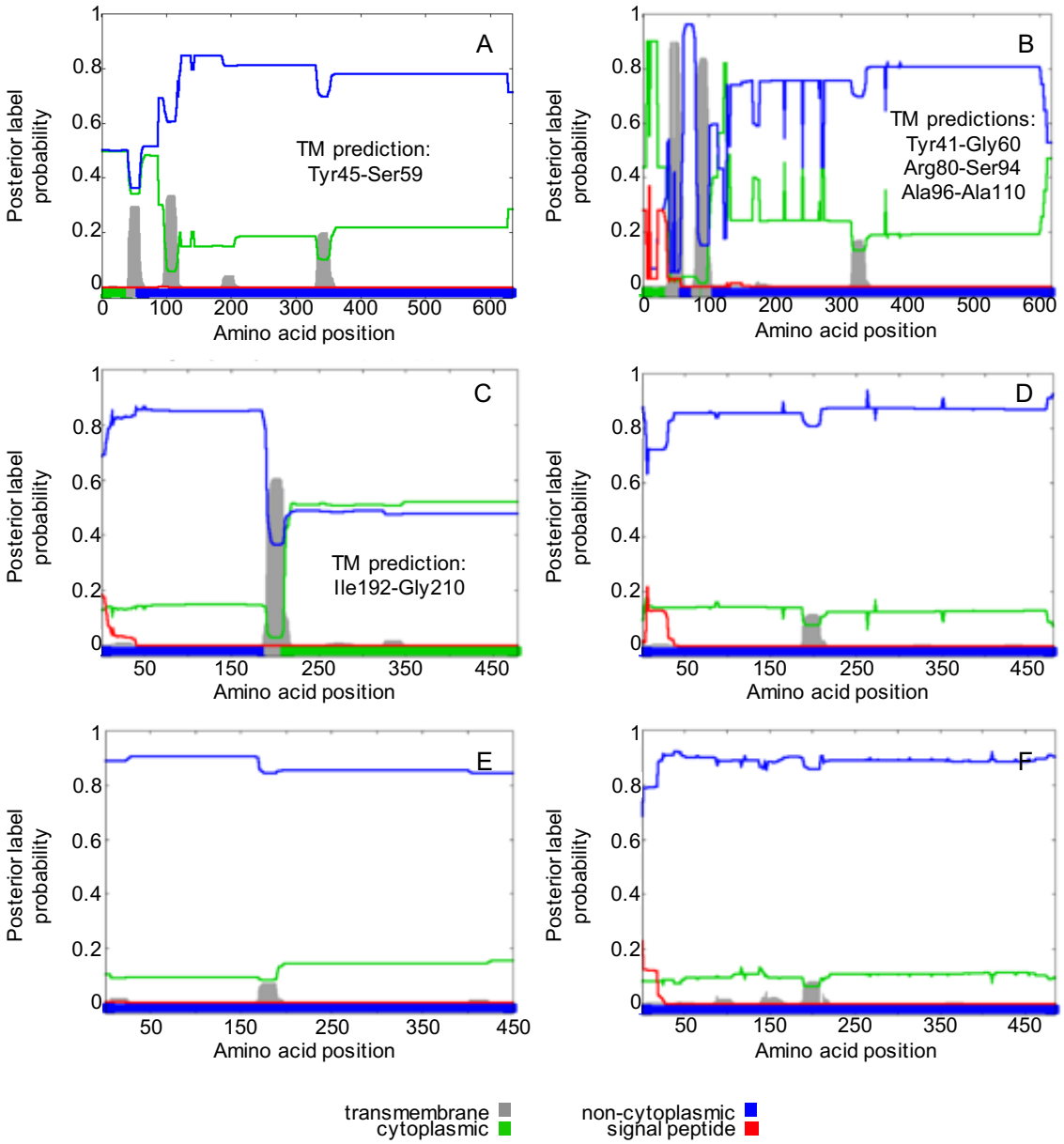

Fig. S9: Transmembrane domains predicted by Polyphobius. ToGR1 (A) and ToGR2 (B) are compared to reference glutathione reductases from *Homo sapiens* (C), *Saccharomyces cerevisiae* (D), *Escherichia coli* (E), and trypanothione reductase from *Trypanosoma cruzi* (F). Each plot shows the posterior probabilities of cytoplasmic, non-cytoplasmic, transmembrane ™ helix, or signal peptide as a function of each amino acid residue in the protein sequence. The overall prediction is indicated by the color stripe at the bottom of each plot. The predicted TM domain in (C) is most likely erroneous, as the amino acids in the indicated positions (Ile192-Gly210) comprise a functional (NADPH-binding) site in the protein (see Fig. S6). TM prediction analysis was performed with Polyphobius (http://phobius.sbc.su.se/poly.html) ref (25).

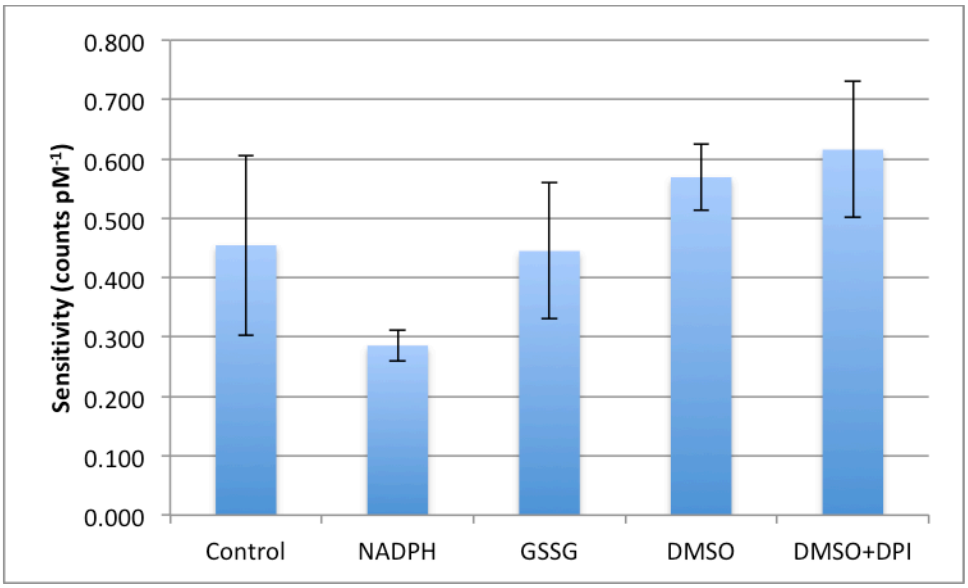

Fig. S10: FeLume sensitivities in the presence of inhibitors and stimulants. The buffered carrier solution was supplemented with NADPH (200μM), GSSG (200μM), DPI (50μM) dissolved in 0.3% DMSO, or 0.3% DMSO (final concentrations). Calibration sensitivities were not significantly affected by these amendments ($p>0.05$, Tukey HSD). Error bars represent one standard deviation of the mean of seven (Control) or three (all others) replicate measurements.

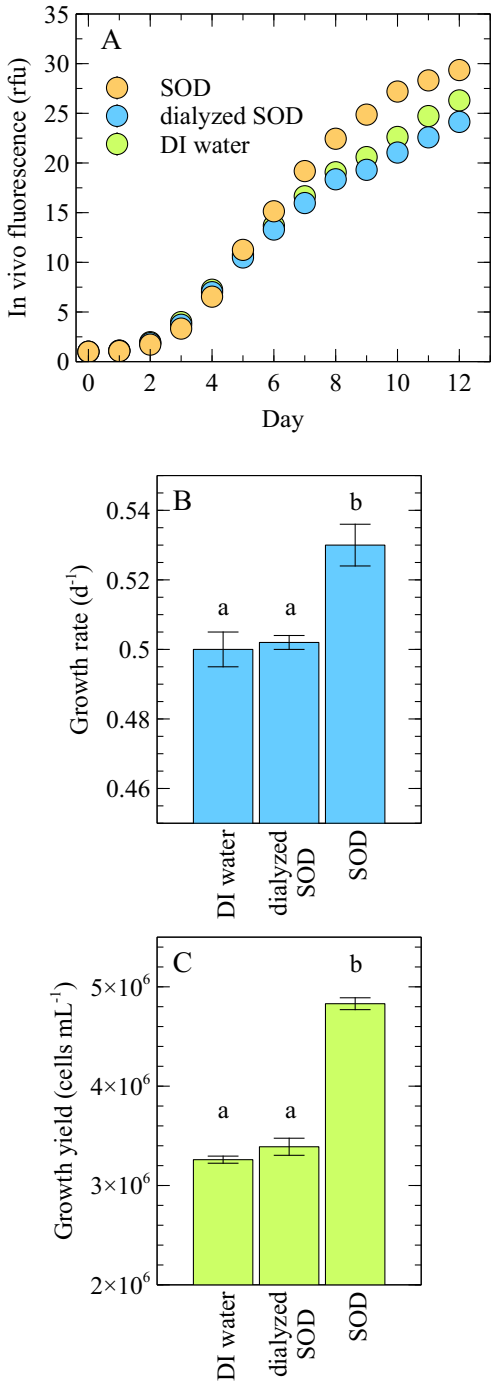

Fig. S11. Growth response of *T. oceanica* to daily additions of SOD. (A) growth curves, (B) specific growth rates during exponential phase, and (C) final cell yields. In all panels, data represent the average ± std. err. of 3 biological replicates. Error bars that are not visible are smaller than the data symbol. Treatments not connected by the same letter are significantly different (Tukey HSD, $p<0.05$). SOD additions were at a final concentration of 50 U mL^{-1}.

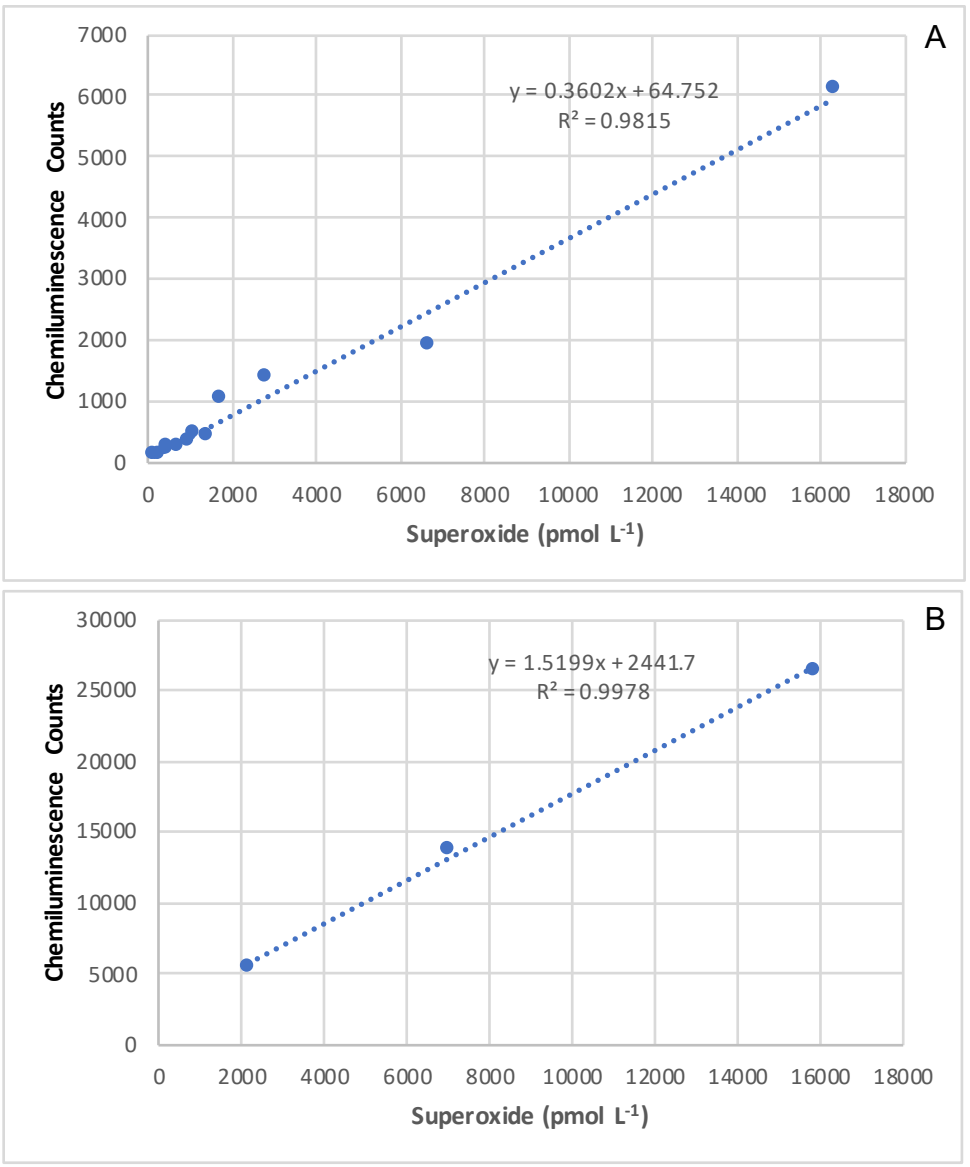

Fig. S12: FeLume standard curves. Standards were analyzed at (A) 30 ms and (B) 100 ms integration time.

References

1. Guillard RRL & Ryther JH (1962) Studies of marine planktonic diatoms. I. *Cyclotella nana* Hustedt and *Detonula confervacea* Cleve. *Can. J. Microbiol.* 8:229-239.
2. Bielski BHJ, Shiue GG, & Bajuk S (1980) Reduction of nitro blue tetrazolium by CO_2^- and O_2^- radicals. *J. Phys. Chem.* 84(8):830-833.
3. Schneider RJ, Roe KL, Hansel CM, & Voelker BM (2016) Species-level variability in extracellular production rates of reactive oxygen species by diatoms. *Frontiers Chem.* 4:5.
4. Andeer PF, Learman DR, McIlvin M, Dunn JA, & Hansel CM (2015) Extracellular haem peroxidases mediate Mn(II) oxidation in a marine *Roseobacter* bacterium via superoxide production. *Environ. Microbiol.* 17(10):3925-3936.
5. Hervé C, Tonon T, Collén J, Corre E, & Boyen C (2005) NADPH oxidases in Eukaryotes: red algae provide new hints! *Curr. Genet.* 49(3):190-204.
6. Pesant S*, et al.* (2015) Open science resources for the discovery and analysis of Tara Oceans data. *Scientific Data* 2:150023.
7. Villar E*, et al.* (2018) The Ocean Gene Atlas: exploring the biogeography of plankton genes online. *Nucleic Acids Research* 46(W1):W289-W295.
8. Pei J, Kim BH, & Grishin NV (2008) PROMALS3D: a tool for multiple protein sequence and structure alignments. *Nucleic Acids Res.* 36(7):2295-2300.
9. Thieme R, Pai EF, Schirmer RH, & Schulz GE (1981) Three-dimensional structure of glutathione reductase at 2 Å resolution. *J. Mol. Biol.* 152(4):763-782.
10. Berkholz DS, Faber HR, Savvides SN, & Karplus PA (2008) Catalytic cycle of human glutathione reductase near 1 Å resolution. *J. Mol. Biol.* 382(2):371-384.
11. Pai EF, Karplus PA, & Schulz GE (1988) Crystallographic analysis of the binding of NADPH, NADPH fragments, and NADPH analogues to glutathione reductase. *Biochemistry* 27(12):4465-4474.
12. Karplus PA & Schulz GE (1989) Substrate binding and catalysis by glutathione reductase as derived from refined enzyme: substrate crystal structures at 2Å resolution. *J. Mol. Biol.* 210(1):163-180.
13. Karplus PA & Schulz GE (1987) Refined structure of glutathione reductase at 1.54 Å resolution. *J. Mol. Biol.* 195(3):701-729.
14. Schulz GE, Schirmer RH, & Pai EF (1982) FAD-binding site of glutathione reductase. *J. Mol. Biol.* 160(2):287-308.
15. Stoll VS, Simpson SJ, KrauthSiegel RL, Walsh CT, & Pai EF (1997) Glutathione reductase turned into trypanothione reductase: Structural analysis of an engineered change in substrate specificity. *Biochemistry* 36(21):6437-6447.
16. Yu J & Zhou CZ (2007) Crystal structure of glutathione reductase Glr1 from the yeast *Saccharamyces cerevisiae*. *Proteins-Structure Function and Bioinformatics* 68(4):972-979.
17. Mittl PRE & Schulz GE (1994) Structure of glutathione reductase from *Escherichia coli* at 1.86 Å resolution: comparison with the enzyme from human erythrocytes. *Protein Sci.* 3(5):799-809.
18. Zhang Y*, et al.* (1996) The crystal structure of trypanothione reductase from the human pathogen *Trypanosoma cruzi* at 2.3 Å resolution. *Protein Sci.* 5:52-61.

19. Taylor MC, Kelly JM, Chapman CJ, Fairlamb AH, & Miles MA (1994) The structure, organization, and expression of the *Leishmania donovani* gene encoding trypanothione reductase. *Mol. Biochem. Parasitol.* 64(2):293-301.
20. Sandalova T, Zhong LW, Lindqvist Y, Holmgren A, & Schneider G (2001) Three-dimensional structure of a mammalian thioredoxin reductase: Implications for mechanism and evolution of a selenocysteine-dependent enzyme. *Proc. Nat. Acad. Sci. U.S.A.* 98(17):9533-9538.
21. Gouy M, Guindon S, & Gascuel O (2009) SeaView Version 4: A Multiplatform Graphical User Interface for Sequence Alignment and Phylogenetic Tree Building. *Mol. Biol. Evol.* 27(2):221-224.
22. Letunic I & Bork P (2019) Interactive Tree Of Life (iTOL) v4: recent updates and new developments. *Nucleic Acids Res.*
23. Grote A, Jahn D, Hiller K, Scheer M, & Münch R (2004) PrediSi: prediction of signal peptides and their cleavage positions. *Nucleic Acids Res.* 32(suppl_2):W375-W379.
24. Persson B & Argos P (1994) Prediction of transmembrane segments in proteins using multiple sequence alignments. *J. Mol. Biol.* 237(182-192).
25. Käll L, Krogh A, & Sonnhammer E (2005) An HMM posterior decoder for sequence feature prediction that includes homology information. *Bioinformatics* 21(Suppl 1):i251-i257.
26. Diaz JM*, et al.* (2013) Widespread production of extracellular superoxide by heterotrophic bacteria. *Science* 340(6137):1223-1226.
27. Zhang T*, et al.* (2016) Dark production of extracellular superoxide by the coral *Porites astreoides* and representative symbionts. *Frontiers Mar. Sci.* 3:232.
28. Hansel CM*, et al.* (2016) Dynamics of extracellular superoxide production by *Trichodesmium* colonies from the Sargasso Sea. *Limnol. Oceanogr.* 61(4):1188-1200.
29. Bielski BHJ, Cabelli DE, & Arudi RL (1985) Reactivity of HO_2/O_2^- Radicals in Aqueous Solution. *J. Phys. Chem. Ref. Data* 14(4):1041-1100.
30. Platt T, Gallegos CL, & Harrison WG (1980) Photoinhibition of photosynthesis in natural assemblages of marine phytoplankton. *J. Mar. Res.* 38:687-701.
31. Hansel CM, Diaz JM, & Plummer S (2019) Tight regulation of extracellular superoxide points to its vital role in the physiology of the globally relevant *Roseobacter* clade. *mBio* 10(2):e02668-02618.
32. Argyrou A & Blanchard JS (2004) Flavoprotein disulfide reductases: advances in chemistry and function. *Prog. Nucleic Acid Res. Mol. Biol.*, ed Moldave K (Elsevier, San Diego, CA), Vol 78, pp 89-142.
33. Deponte M (2013) Glutathione catalysis and the reaction mechanisms of glutathione-dependent enzymes. *Biochim. Biophys. Acta* 1830:3217-3266.
34. Fujimori K*, et al.* (1993) Chemiluminescence of *Cypridina* luciferin analogues. Part 1. Effect of pH on rates of spontaneous autoxidation of CLA in aqueous buffer solutions. *Journal of the Chemical Society-Perkin Transactions 2* (12):2405-2409.
35. Lin PC, Turk K, Hase CC, Fritz G, & Steuber J (2007) Quinone reduction by the Na^+-translocating NADH dehydrogenase promotes extracellular superoxide production in *Vibrio cholerae*. *J. Bacteriol.* 189(10):3902-3908.
36. Korshunov S & Imlay JA (2006) Detection and quantification of superoxide formed within the periplasm of *Escherichia coli*. *J. Bacteriol.* 188(17):6326-6334.

934 37. Fisher AB (2009) Redox Signaling Across Cell Membranes. *Antioxidants & Redox*
935 *Signaling* 11(6):1349-1356.
936 38. Diaz JM & Plummer S (2018) Production of extracellular reactive oxygen species by
937 phytoplankton: past and future directions. *J. Plankton Res.* 40(6):655-666.
938 39. Cardol P, Forti G, & Finazzi G (2011) Regulation of electron transport in microalgae.
939 *Biochim. Biophys. Acta Bioenerg.* 1807(8):912-918.
940 40. Bräutigam A & Weber APM (2011) Do Metabolite Transport Processes Limit
941 Photosynthesis? *Plant Physiol.* 155(1):43-48.
942